Supplementary Information

Multifunctional molecules with bipyridyl core ameliorate multifaceted amyloid toxicity

Dikshaa Padhi[a], Chenikkayala Balachandra[a], Madhu Ramesh[a] and Thimmaiah Govindaraju[a*]

[a] Bioorganic Chemistry Laboratory, New Chemistry Unit Jawaharlal Nehru Centre for Advanced Scientific Research (JNCASR) Jakkur P.O., Bengaluru 560064, Karnataka, India.

* E-mail: tgraju@jncasr.ac.in

Table of contents

1. Materials and method

All the starting materials, reagents, and solvents were obtained from Merck and Spectrochem and used without any further purification unless otherwise mentioned. Moisture sensitive reactions were carried out under nitrogen atmosphere. $A\beta_{42}$ peptide was purchased from Invitrogen (Cat: 03112-1mg), which was dissolved in 1 mL of hexafluoro-2-propanol (HFIP). Post sonication under ice-cold conditions, HFIP was first removed by nitrogen gas flow and then under vacuum condition. $A\beta_{42}$ peptide concentration was calculated by UV-visible absorbance by using $A\beta_{42}$ molar extinction coefficient 1450 cm^{-1} M^{-1}.OC primary antibody, Thioflavin T (ThT), *E. coli* lipopolysachharide (LPS), Greiss reagent, 2,2-diphenyl-1-picrylhydrazyl (DPPH), 2,2'-azino-bis(3-ethylbenzothiazoline-6-sulphonic acid (ABTS), dichlorodihydrofluorescein diacetate (DCFDA), ascorbate, 3-(4,5-dimethylthiazol-2-yl)-2,5-diphenyltetrazolium bromide (MTT), xylenol orange were procured from Merck. Enhanced chemiluminescence (ECL) reagent and PVDF membrane were purchased from BioRad. Sterile plastic wares for cell culture were purchased from ThermoFischer Scientific. Dulbecco′s Modified Eagle′s Medium (DMEMF12) media, fetal bovine serum (FBS), penicillin streptomycin (PS), horse serum (HS) and trypsin were purchased from Gibco (ThermoFischer Scientific). Agilent Cary series UV-Vis-NIR absorption, and Agilent Cary eclipse fluorescence spectrophotometers and Spectra Max 3i microplate reader (Molecular Devices) were used for all absorption and fluorescence measurements ^{1}H and ^{13}C NMR of all synthesized compounds were recorded using Bruker AV-400 spectrometer and tetramethylsilane as an internal standard. High resolution-mass spectra (HR-MS) were acquired on Agilent 6538 UHD HR-MS/Q-TOF high resolution spectrometer. The electrochemical experiments were performed using CHI 832 electrochemical workstation (CH Instruments, Austin, Texas). The EPR spectra was recorded in a JEOL, JES-X320 EPR spectrometer. The atomic force microscopy (AFM) was performed in Bioscope Resolve (Bruker). The main stock solutions of all the compounds were prepared by dissolving the calculated amount of corresponding solids in DMSO, and stored in -20 ℃. Stock solutions of Cu^{2+}, Fe^{3+} and Zn^{2+} samples were obtained by dissolving the calculated amount of copper sulphate ($CuSO_4$), ferric chloride ($FeCl_3$) and Zinc chloride ($ZnCl_2$) in deionized water (Milli Q). All the raw data was processed and analysed in Prism 5, OriginPro 2016 and ImageJ softwares.

2. Synthesis of compounds 1-9. The commercially available 2,2′-bipyridyl-5,5′-dicarboxylic acid (100 mg, 0.40 mmol) was dissolved in dimethylformamide (1.5 mL) and methylene chloride (0.5 mL) and was sonicated to obtain a clear solution. It was cooled to 0 ℃ under nitrogen atmosphere for 5 min. DIPEA (417 μL, 2.40 mmol) was added and stirred for 5 min. HBTU (363.84 mg, 0.96 mmol) was added and reaction mixture was stirred at 0 ℃ for 15 min. To the reaction mixture, the appropriate functional moiety was added, viz., dopamine and methyl esters of L-Tyrosine, L-Tryptophan, L-Dopa and alanine, and the reaction mixture was allowed to stir at ice cold to room temperature for 6 h, to obtain **1-5**. Compounds **6-9** were obtained by dissolving their respective esters in THF:MeOH (1:1) and stirred for 5 min, followed by the addition of LiOH (7.42 mg, 0.31 mmol) and stirred for 1 h. The purity of the hydrolysed products was monitored by thin layer chromatography (TLC), followed by evaporation of volatiles under reduced pressure. The hydrolysed products (**6-9**) were acidified by the addition of 1N HCl and pelleted down by centrifugation. All the compounds (**1-9**) were purified by column chromatography and the integrity of the final compounds was confirmed by ^{1}H NMR, ^{13}C NMR and HR-MS analysis.

Compound 1. Yield 81% (190 mg); colourless solid; R_f 0.4 (MeOH/DCM = 0.5:9.5) ^{1}H NMR (400 MHz, DMSO-d_6) δ 9.22 (s, 2H), 9.14 (d, J = 7.8 Hz, 2H), 9.06 (d, J = 2.2 Hz, 2H), 8.52 (d, J = 8.3 Hz, 2H), 8.33 (dd, J = 8.3, 2.3 Hz, 2H), 7.10 (d, J = 8.5 Hz, 4H), 6.67 (d, J = 8.5 Hz, 4H), 4.63 (ddd, J = 10.0, 7.7, 5.4 Hz, 2H), 3.65 (s, 6H), 3.08 (dd, J = 13.8, 5.4 Hz, 2H), 2.98 (dd, J = 13.8, 9.9 Hz, 2H). ^{13}C NMR (100 MHz, DMSO-d_6) δ 172.1, 164.8, 156.6, 156.0, 148.5, 136.5, 130.0, 129.5, 127.4, 120.8, 115.0, 54.7, 52.0, 35.8. HRMS (ESI-MS): m/z calcd for $C_{32}H_{30}N_4O_8$ $[M+H]^+$ 599.2136, found 599.2100.

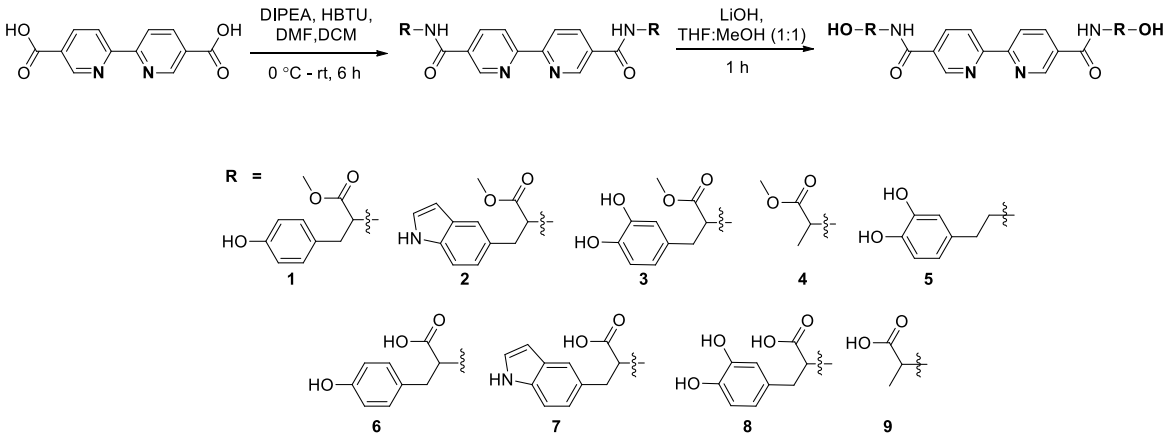

Scheme S1. Synthesis of bipyridine derivatives **1-9**.

Compound 3. Yield 63.4% (161 mg); colourless solid; R_f 0.3 (MeOH/DCM = 0.5:9.5) ^{1}H NMR (400 MHz, DMSO-d$_6$) ^{1}H NMR (400 MHz, DMSO-*d*$_6$) δ 9.13 (d, *J* = 7.7 Hz, 2H), 9.08 (d, *J* = 1.9 Hz, 2H), 8.52 (d, *J* = 8.2 Hz, 2H), 8.36 (d, *J* = 2.2 Hz, 1H), 8.34 (d, *J* = 2.2 Hz, 1H), 6.68 (d, *J* = 1.9 Hz, 2H), 6.62 (d, *J* = 8.0 Hz, 2H), 6.55 (d, *J* = 1.9 Hz, 1H), 6.53 (d, *J* = 1.9 Hz, 1H), 4.60 (d, *J* = 5.6 Hz, 2H), 3.65 (s, 6H), 3.01 (dd, *J* = 13.8, 5.4 Hz, 2H), 2.92 (dd, *J* = 13.8, 9.8 Hz, 2H). ^{13}C NMR (100 MHz, DMSO-*d*$_6$) δ 171.9, 164.5, 156.4, 148.6, 145.1, 144.0, 136.6, 129.7, 128.1, 120.5, 119.8, 116.4, 115.1, 54.8, 52.1, 35.9. HRMS (ESI-MS): m/z calcd for $C_{32}H_{30}N_4O_{10}$ $[M+H]^+$ 631.2035, found 631.2025.

Compound 4. Yield 75.48% (125.3 mg); colourless solid; R_f 0.6 (MeOH/DCM = 0.5:9.5) ^{1}H NMR (400 MHz, DMSO-*d*$_6$) δ 9.17 (d, *J* = 10.8 Hz, 2H), 9.14 (d, *J* = 6.9 Hz, 2H), 8.55 (d, *J* = 8.3 Hz, 2H), 8.43 (s, 1H), 8.43 (d, *J* = 6.2 Hz, 1H), 4.54 (s, 2H), 3.67 (s, 6H), 1.44 (d, *J* = 7.3 Hz, 6H). ^{13}C NMR (101 MHz, DMSO-*d*$_6$) δ 172.89, 164.47, 156.46, 148.65, 136.55, 129.52, 120.58, 51.96, 48.31, 40.18, 40.13, 39.92, 39.71, 39.50, 39.29, 39.08, 38.87, 16.68, 0.06. HRMS (ESI-MS): m/z calcd for $C_{20}H_{22}N_4O_6$ $[M+H]^+$ 415.1539, found 415.1616.

Compound 5. Yield 70.6% (145.6 mg); colourless solid; R_f 0.3 (MeOH/DCM = 0.5:9.5) ^{1}H NMR (600 MHz, DMSO-d$_6$) ^{1}H NMR (600 MHz, DMSO-*d*$_6$) δ 9.11 (d, *J* = 2.2 Hz, 2H), 8.85 (t, *J* = 5.6 Hz, 2H), 8.79 (s, 2H), 8.68 (s, 2H), 8.53 (d, *J* = 8.3 Hz, 2H), 8.36 (dd, *J* = 8.2, 2.3 Hz, 2H), 6.69 – 6.64 (m, 4H), 6.51 (dd, *J* = 8.0, 2.2 Hz, 2H), 3.48 – 3.44 (m, 4H), 2.71 (t, *J* = 7.5 Hz, 4H).^{13}C NMR (150MHz, DMSO-*d*$_6$) δ 164.2, 156.2, 148.3, 145.0, 143.5, 136.2, 130.4, 130.1, 120.4, 119.2, 116.0, 115.5, 41.3, 40.0, 39.9, 39.7, 39.6, 39.5, 39.3, 39.2, 39.0, 34.4. HRMS (ESI-MS): m/z calcd for $C_{28}H_{26}N_4O_6$ $[M+H]^+$ 515.1931, found 515.1910.

Compound 6. Yield 75% (175 mg); colourless solid; R_f 0.2 (MeOH/DCM = 0.5:9.5) ^{1}H NMR (400 MHz, DMSO-*d*$_6$) δ 9.06 (d, *J* = 2.3 Hz, 2H), 9.02 (d, *J* = 8.1 Hz, 2H), 8.51 (d, *J* = 8.3 Hz, 2H), 8.34 (dd, *J* = 8.3, 2.3 Hz, 2H), 7.12 (d, *J* = 8.5 Hz, 4H), 6.66 (d, *J* = 8.5 Hz, 4H), 4.60 – 4.55 (m, 2H), 3.10 (dd, *J* = 13.8, 4.6 Hz, 2H), 3.01 – 2.91 (m, 2H). ^{13}C NMR (101 MHz, DMSO-*d*$_6$) δ 173.15, 164.69, 156.42, 156.05, 148.63, 136.75, 130.17, 130.05, 128.11, 120.83, 115.19, 54.81, 40.33, 40.12, 39.96, 39.91, 39.70, 39.49, 39.28, 39.08, 35.78. HRMS (ESI-MS): m/z calcd for $C_{30}H_{26}N_4O_8$ $[M+H]^+$ 571.1751, found 571.1737

Compound 7. Yield 85.3% (210 mg); colourless solid; R_f 0.2 (MeOH/DCM = 0.5:9.5 ^{1}H NMR (400 MHz, DMSO-*d*$_6$) δ 10.75 (d, *J* = 2.4 Hz, 2H), 9.02 (d, *J* = 2.2 Hz, 2H), 8.64 (d, *J* = 7.7 Hz, 2H), 8.45 (d, *J* = 8.3 Hz, 2H), 8.27 (dd, *J* = 8.3, 2.2 Hz, 2H), 7.59 (d, *J* = 7.9 Hz, 2H), 7.30 (d, *J* = 8.1 Hz, 2H), 7.17 (d, *J* = 2.3 Hz, 2H), 7.03 (t, *J* = 7.5 Hz, 2H), 6.94 (t, *J* = 7.4 Hz, 2H), 4.56 (td, *J* = 8.1, 4.4 Hz, 2H),

3.18 (dd, J = 14.7, 8.7 Hz, 5H). ^{13}C NMR (100 MHz, DMSO-d_6) δ 173.6, 163.8, 156.0, 148.0, 136.0, 135.7, 130.3, 127.4, 123.1, 120.4, 120.1, 118.2, 117.9, 111.0, 55.0, 27.1. HRMS (ESI-MS): m/z calcd for $C_{34}H_{28}N_6O_6$ $[M+H]^+$ 617.2143, found 617.2096.

Compound 8. Yield 64.2% (155 mg); colourless solid; R_f 0.2 (MeOH/DCM = 0.5:9.5) ^{1}H NMR (400 MHz, DMSO-d_6) δ 13.22 (s, 2H), 9.25 – 9.15 (m, 2H), 9.08 (d, J = 2.2 Hz, 1H), 8.99 (d, J = 8.0 Hz, 1H), 8.59 – 8.50 (m, 3H), 8.44 (ddd, J = 8.3, 3.9, 2.2 Hz, 2H), 8.35 (dd, J = 8.2, 2.3 Hz, 1H), 7.96 (d, J = 8.4 Hz, 1H), 7.71 (d, J = 8.4 Hz, 1H), 7.51 (t, J = 7.6 Hz, 1H), 7.39 (t, J = 7.7 Hz, 1H), 7.27 – 7.07 (m, 1H), 6.70 (d, J = 2.0 Hz, 1H), 6.62 (d, J = 8.0 Hz, 1H), 6.58 – 6.53 (m, 1H), 4.75 – 4.44 (m, 2H), 3.02 (dt, J = 14.8, 7.5 Hz, 2H), 2.89 (dd, J = 13.8, 10.1 Hz, 2H). ^{13}C NMR (100 MHz, DMSO-d_6) δ 173.05, 166.04, 150.27, 148.62, 144.95, 143.81, 138.44, 136.62, 130.05, 128.68, 126.97, 119.82, 116.40, 115.36, 54.67, 39.91, 39.78, 39.64, 39.50, 39.36, 39.22, 39.08, 35.84. HRMS (ESI-MS): m/z calcd for $C_{30}H_{26}N_4O_{10}$ $[M+H]^+$ 603.1722, found 603.1697.

Compound 9. Yield 82.4% (127 mg); colourless solid; R_f 0.4 (MeOH/DCM = 0.5:9.5) ^{1}H NMR (400 MHz, DMSO-d_6) δ 12.65 (s, 2H), 9.16 (d, J = 1.6 Hz, 2H), 9.01 (d, J = 7.2 Hz, 2H), 8.55 (d, J = 8.3 Hz, 2H), 8.44 (d, J = 2.2 Hz, 1H), 8.42 (d, J = 2.2 Hz, 1H), 4.47 (s, 2H), 1.44 (d, J = 7.3 Hz, 6H). ^{13}C NMR (101 MHz, DMSO-d_6) δ 174.23, 164.70, 156.56, 148.96, 136.68, 130.05, 120.83, 48.51, 40.33, 40.13, 39.92, 39.71, 39.50, 39.29, 39.08, 17.20. HRMS (ESI-MS): m/z calcd for $C_{18}H_{18}N_4O_6$ $[M+H]^+$ 387.1300, found 387.1338.

3. Absorption spectroscopy. UV-vis spectroscopy measurements were carried out using single beam Agilent 8453 UV-Vis spectrophotometer at room temperature. Quartz cuvette of 1 cm path length (1 mL) was used for the absorbance measurement (200-800 nm). The metal-binding property of compounds **1-9 (**freshly prepared 10 mM stock solution in DMSO) was carried out in PBS buffer (10 mM, pH= 7.4). We titrated with increasing concentration of metal ions (Cu^{2+}/Zn^{2+}) ranging from 0.1 μM to 50 μM into the compound solutions, with 5 min incubation after each titration, and recorded the changes in absorbance spectra. Distinct shifts in wavelengths and absorbance intensity were observed for some of the compounds, which indicated their binding to specific metal ions. The raw data from the metal-binding studies were analysed using Origin 8.0 software. The data was fitted to non-linear curve and Boltzmann function to obtain the K_d values of compounds **1-9** in the presence of metal ions.
Both bipyridine and catechols are potent metal ion binders. To study their individual binding interaction with metal ions, we studied the changes in absorbance spectra in the presence of bipyridine, subsequently followed by pyrocatechol, dopamine, L-dopa and Cu^{2+}, each at 10 μM. On addition of catechols to the bipyridine-Cu^{2+} solution, distinct changes in absorbance was observed, which clearly indicate the role of catechols in metal-binding. Thus, our compounds **1-9** with bipyridine and catechols (covalently conjugated) units exhibit synergism in metal-binding.

4. Monitoring the oxidation of catechol moiety. To study whether catechol moiety present in compounds (**3**, **5** and **8**) reduce Cu^{2+} and oxidize itself, we titrated Cu^{2+} in a concentration-dependant manner (0.1 μM to 50 μM) into a solution containing pyrocatechol (50 μM) and recorded the changes in absorbance spectra. A broad absorption band at 400 nm was observed with increasing concentration of Cu^{2+}, which attributes to the oxidation of catechols.[1] However, in case of compounds **3**, **5** and **8**, no absorbance band at 400 nm is observed which possibly indicates the absence of oxidation of catechol moieties in these compounds.

5. $A\beta_{42}$ Aggregation inhibition. $A\beta_{42}$ peptide was dissolved in PBS buffer (10 mM, pH= 7.4) containing 1% DMSO to obtain a final concentration of 10 μM, which is used as a stock solution. To evaluate the $A\beta_{42}$ aggregation inhibition ability of bipyridine compounds, ThT assay was performed.

Freshly reconstituted $A\beta_{42}$ (10 μM) was incubated alone and with compounds (10 μM) in phosphate buffer saline (PBS, pH=7.4 and 10 mM) at 37 °C for 48 h. Filtered PBS (pH= 7.4, 10 mM) was used to dissolve the calculated amount of ThT. Finally, ThT (10 μM) was added to the respective samples and left for 10 min incubation. ThT fluorescence emission intensity was measured at 482 nm (λ_{ex} = 442 nm) using microplate reader and data was plotted analysed by GraphPad Prism 5 software.

6. Dot blot analysis. The inhibitory activity of bipyridine compounds (**1-9**) against metal-independent $A\beta_{42}$ fibrillar aggregates, was evaluated using dot blot analysis. Freshly prepared $A\beta_{42}$ sample (10 μM) was incubated alone, and with compounds **1-9** (10 μM) in PBS for 24 h with shaking. For analysis of dissolution ability of compounds, freshly prepared $A\beta_{42}$ samples were incubated alone for 48 h to prepare fibrils. Then compounds **1-9** (10 μM) were treated and further incubated for 48 h. The respective samples were spotted onto the PVDF membrane, and the membrane was blocked with 5% skimmed milk powder in tris-buffered saline with Tween-20 (TBST) for 1 h. This was followed by three times washing with TBST for 5 min each. The membrane was incubated with $A\beta_{42}$ fibrils specific primary antibody (OC, Merck Millipore) at 4 °C for 18 h, followed by the treatment with HRP-conjugated secondary antibody (1:5000), for 1 h. Finally, the membrane was developed with ECL reagent (Biorad) and blot imaged in Biorad ChemiDoc imaging instrument. The blot was quantified by ImageJ and analysed by GraphPad Prism 5 software.

7. MTT assay. Cytotoxicity of compounds was assessed by performing MTT assay in SHSY-5Y cell lines. 20,000 cells/well were seeded in a 96-well plate in DMEM F12 with 10% FBS, 5% HS, and 1% PS and incubated at 37 °C with 5% CO_2 atmosphere for 24 h. Different concentrations of compounds (25, 50, 100, 150 and 200 μM) was treated and incubated for 24 h under similar conditions. Then 10 μL of MTT solution (5 mg/mL) was added to each well, media was removed and 1:1 DMSO-MeOH (100 μL) was added after 3 h of incubation. The absorbance was measured at 570 nm and 630 nm after 30 min of shaking in the dark. The absorbance measurement was carried out using a microplate reader, and the data was plotted and analysed by GraphPad Prism 5 software.

8. Atomic force microscopy (AFM) imaging. Samples were drop casted on freshly cleaved mica discs (TedPella), allowed at room temperature for 15 min and rinsed twice with filtered MQ water for 5 min. The sample was left for drying for 30 min at 37 ℃. Samples were imaged in AFM (Bruker Bioscope resolve) using SCANASYST-AIR probe with tip radius of 5 nm and spring constant 0.4 N/m with scanned speed of 1Hz. The data processing and analysis of images was done using NanoScope analysis 1.8 software (Bruker).

9. Antioxidant assays

DPPH radical scavenging assay. DPPH radical quenching assay was performed to demonstrate the radical scavenging ability (RSA) of compounds **1-9**. DPPH (100 μM) was incubated alone or with different concentration of compounds (1, 2, 5, 10, 20, 50, 75, 100 μM) in MeOH:H_2O (1:1) at 37 °C for 30 min. The absorbance at 540 nm was measured using microplate reader and data was plotted and analysed by GraphPad Prism 6 software. The DPPH assay was performed in the presence of catechols, bipyridine and their combinations (physical mixture). In this assay, pyrocatechol, L-dopa and dopamine showed EC_{50} values of 29.87, 10.87 and 37.90 μM, respectively. The physical mixtures of pyrocatechol, L-dopa and dopamine with bipyridine exhibited EC_{50} values of 21.49, 6.58, and 7.185 μM respectively. These results indicate that our compounds **3**, **5** and **8** show improved RSA as compared to the physical mixtures of bipyridine and catechols.

ABTS radical scavenging assay. The reactive nitrogen species (RNS) radical scavenging ability of compounds **3**, **5** and **8** was measured using 2,2'-azinobis-(3-ethylbenzothiazoline-6-sulfonic acid (ABTS) assay. On reaction of ABTS and potassium persulfate for 12 h, deep green coloured ABTS radical cation ($ABTS^{\cdot+}$) was formed. $ABTS^{\cdot+}$ (100 μM) was incubated alone or with different concentrations of compounds **3, 5** and **8** in PBS at 37 °C for 30 min. The absorbance at 734 nm was

measured using microplate reader and data was plotted and analyzed by GraphPad Prism 5 software. Pyrocatechol, dopamine and L-dopa in combination (physical mixture) with bipyridine showed EC_{50} values of 17.52, 13.30, and 6.47 μM, respectively, which indicates the efficient RSA of compounds **3**, **5** and **8** over the physical mixtures of bipyridine and catechols.

FOX assay. The decreasing peroxide concentrations in presence of compounds **3**, **5** and **8** were measured using Fe^{2+} and xylenol orange (XO). Under acidic conditions, peroxides oxidize Fe^{2+} to Fe^{3+}, which eventually forms a complex with XO that absorbs maximum at 550 nm. Compounds **3**, **5**, and **8** at increasing concentrations of 0.1, 0.5, 1, 5 and 10 μM were added to the reaction mixture consisting of 100 μL of ferrous ammonium sulfate (50 mM), 200 μL methanolic H_2SO_4 (0.2 M) and 200 μL methanolic xylenol orange (1 mM) in ethanolic medium, and change in absorbance was recorded using microplate reader and data was plotted and analysed by GraphPad Prism 5 software.

PFRAP assay. PFRAP assay was employed to measure the Fe^{3+} reducing potential of bipyridine compounds **3**, **5** and **8** by the reaction with potassium ferricyanide ($K_3[Fe(CN)_6]$) to form potassium ferrocyanide ($K_4[Fe(CN)_6]$). Then 1% potassium ferricyanide (30 μL) was added to 10 mM PBS (pH 6.6), followed by addition of compounds **3**, **5**, **8** and ascorbate at concentrations of 0.1, 0.5, 1, 5, and 10 μM. This was followed by incubation at 50 °C for 20 min and 30 μL of 10% trichloroacetic acid was added to each well. The absorbance was measured at 700 nm to calculate FRAP capacity of compounds. In this assay, pyrocatechol, dopamine, L-dopa and bipyridine at 10 μM concentration indicated PFRAP activities of 58%, 60%, 85% and 36%, respectively. However, covalent conjugates **3**, **5** and **8** showed improved PFRAP activity as compared to individual catechols and bipyridine components, which reiterates the enhanced and synergistic effect upon covalent conjugation (**3**, **5** and **8**).

Redox silencing of Cu^{2+}. To access the generation of ROS, if any, in the presence of our compounds **3**, **5** and **8**, we performed *in vitro* redox-silencing assay. $A\beta_{42}$ (10 μM) in the presence of Cu^{2+} (10 μM) and dopamine (100 μM) in 10 mM PBS (pH= 7.4) was incubated with and without compounds **3**, **5** and **8** (100 μM), followed by addition of coumarin-3-carboxylic acid (3-CCA, 150 μM) at 37 °C.

The transformation of non-fluorescent 3-CCA to fluorescent 7-OH-CCA (λ_{ex} = 385 nm, λ_{em} = 450 nm) was used to assess the •OH generation, over a period of 90 min. Samples incubated with Cu^{2+}-$A\beta_{42}$ in the absence of our compounds showed maximum 7-HO-CCA fluorescence emission (100%). However, compounds **3** and **5** showed considerably reduced fluorescence emission (< 10%), while compound **8** showed ~20% fluorescence emission. These results indicate the ability of compounds **3** and **5** to chelate Cu^{2+} and keep it in the redox-dormant state, thus preventing the ROS generation.

10. Intracellular ROS measurement. To demonstrate the *in cellulo* ROS scavenging ability of bipyridine compounds, 2′,7′-dichlorofluorescin diacetate (DCFDA) assay was performed in SHSY-5Y cells. Cells were seeded in a 48-well plate (50,000 cells per well) in DMEM F12 medium (Gibco, Invitrogen) with 10% FBS and 1% PS at 37 °C temperature within 5% CO_2 atmosphere. The cultured media was exchanged with low serum DMEM F12 media (2.5% FBS) and incubated with DCFDA (10 μM) for 30 min. The cells were washed with PBS followed by treatment with H_2O_2 (50 μM) alone and in the presence of compounds (10 μM). After 4 h, the media was removed, cells were washed with PBS (3 times) and the total fluorescence (λ_{em}= 530 nm) of the entire well was measured using microplate reader in well scan mode.

11. *In Cellulo* radical scavenging assay. To evaluate the radical scavenging ability of compounds in cellular context, cell rescue assay was performed with H_2O_2. Cells were cultured in a 96-well plate (15,000 per well) in DMEM F12 medium with FBS (10%), and pen-strep (1%). The cultured media was exchanged with low serum DMEM F12 (2.5% FBS) and cells were treated with H_2O_2 (150 μM) in the absence and presence of compounds **3, 5** and **8** at 10, 20 and 50 μM for 24 h. The cell viability was determined by MTT assay.

12. Nitric oxide assay. To check the reduction in nitric oxide levels in the presence of bipyridine compounds, Griess assay was performed in C6 glial cells. C6 cells were cultured in DMEMF12 medium with 10% FBS, 5% HS, and 1% PS at 37 °C temperature within 5% CO_2 atmosphere. The cultured media was exchanged with low serum phenol red free DMEM F12 media (2.5% FBS) and cells were treated with LPS (2.5 μM) in the absence and presence of bipyridine compounds (10 μM) for 24 h. Next, Griess reagent was added to culture media and incubated on a shaker for 30 min in the dark. The absorbance at 530 nm was measured to calculate the relative NO levels.

13. Modulation of $A\beta_{42}$ toxicity in cells. To demonstrate the modulation of $A\beta_{42}$ toxicity by bipyridine compounds, *in cellulo* assay was performed with SHSY-5Y cells using monomeric and fibrillar $A\beta_{42}$. SHSY-5Y cells were cultured in a 96-well plate (15,000 per well) in DMEM F12 medium (Gibco, Invitrogen). The cultured media was exchanged with low serum DMEM F12 media (2.5% FBS) and cells were treated with $A\beta_{42}$ in the absence and presence of compounds for 24 h. For fibrils modulation assay, cells treated with metal-independent and dependent monomeric or fibrillar $A\beta_{42}$ were incubated with compounds for 24 h and the cell viability was determined by MTT assay.

14. Gel electrophoresis and Western blotting. For analysis of metal-dependant (Cu^{2+}/Zn^{2+}) $A\beta_{42}$ aggregation modulation by compounds **1**-**9**, we performed native-PAGE followed by Western blotting. $A\beta_{42}$ (10 μM) in the presence of Cu^{2+}/Zn^{2+} (10 μM) treated with compounds (10 μM) was incubated for 30 h, in HEPES buffer, 10 mM, pH = 7.4 (Cu^{2+}), pH = 6.8 (Zn^{2+}). Post 30 h incubation, 10 μL of each sample was loaded onto a 6% gel for 1 h 30 min. Following separation, the proteins were transferred onto the PVDF membrane, and developed similar to dot blot.

15. Tyrosine fluorescence assay. To understand the efficient Cu^{2+} sequestration property of lead compound **5**, the intrinsic tyrosine (Tyr^{10}) fluorescence of $A\beta_{42}$ was monitored using fluorescence spectroscopy (λ_{ex} = 285 nm, λ_{em}= 308 nm). $A\beta_{42}$ (10 μM) was left for incubation in PBS (10 mM, pH = 7.4) and Cu^{2+} (10 μM) for 10 min, which was followed by the addition of compound **5** at increasing concentrations of 10, 15, 17.5 and 20 μM. The control experiments were carried out by monitoring the fluorescence due to increasing concentration of **5**, with and without Cu^{2+}, and in the presence of $A\beta_{42}$ (10 μM). Compound **5** alone and upon titration with Cu^{2+} displayed basal fluorescence which infers that compound **5** and its Cu^{2+}complex do not interfere with $A\beta_{42}$ Tyr fluorescence. The fluorescence intensities obtained on titration with increasing concentration of compound **5** into $A\beta_{42}$ solution was similar to intrinsic Tyr_{10} fluorescence present in $A\beta_{42}$. These control experiments confirm the strong Cu^{2+} sequestration property of compound **5** from $A\beta_{42}$-Cu^{2+} complex.

16. Results

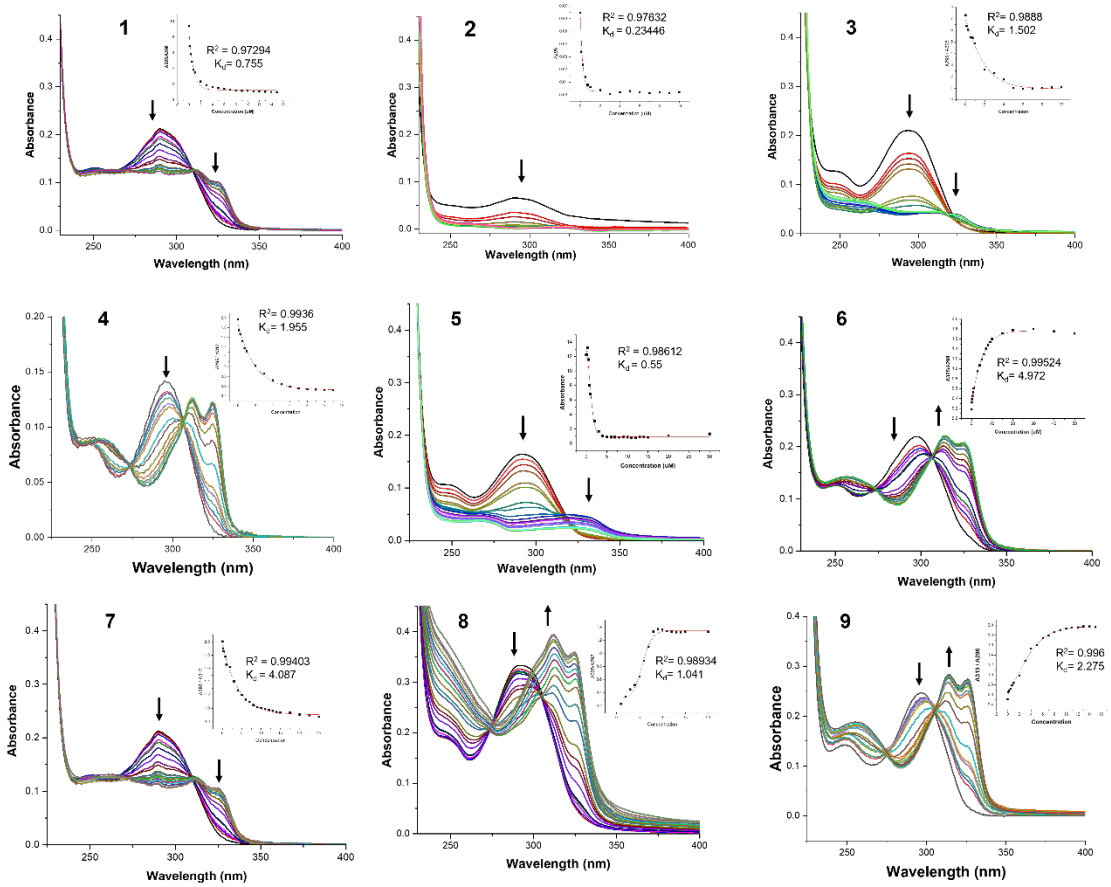

Fig. S1 Copper chelation study. Absorption spectra and their analysis (insets) of compounds **1-9** treated with Cu^{2+} at increasing concentrations of 0.1 μM to 20 μM.

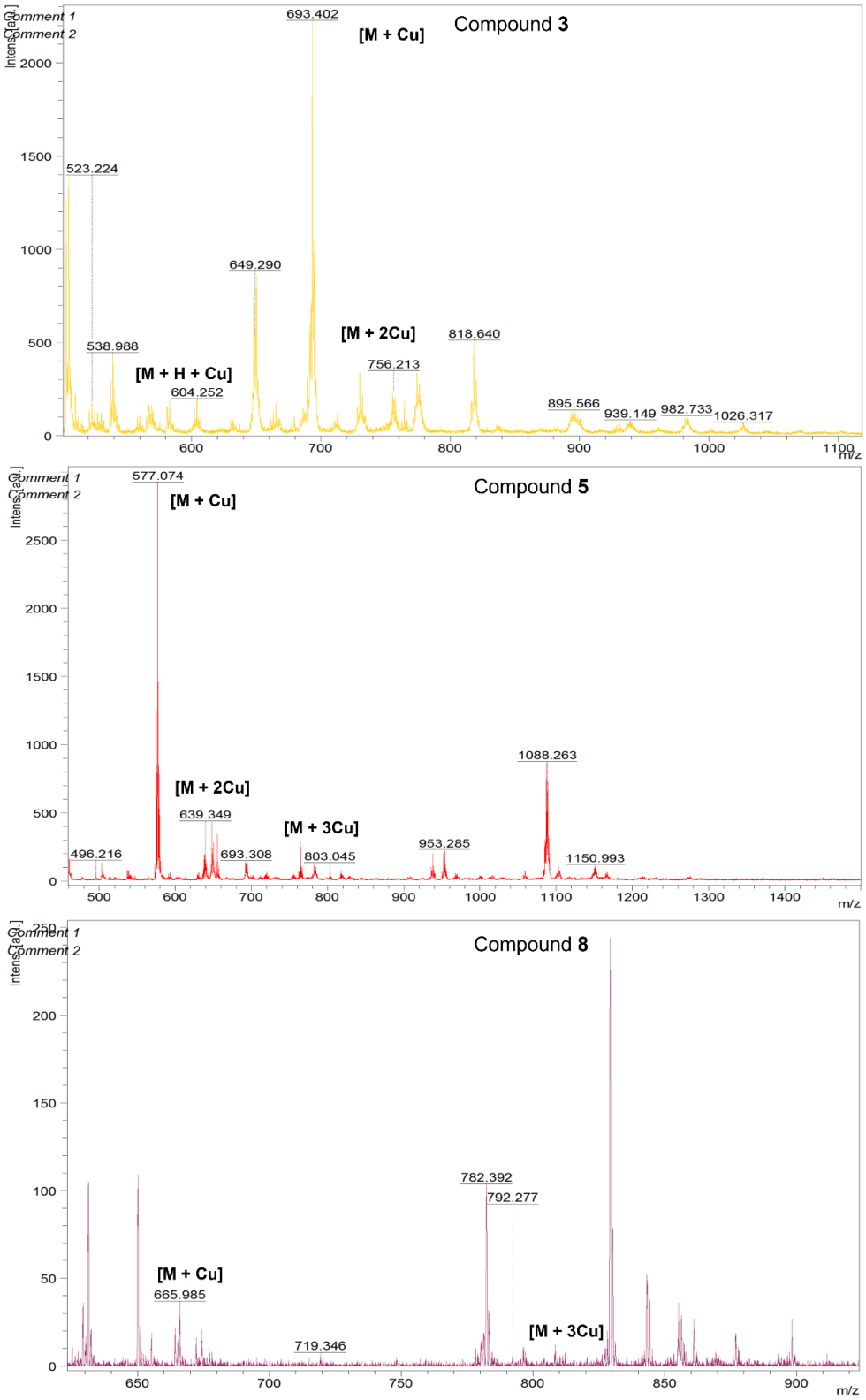

Fig. S2 MALDI analysis of compound **3, 5** and **8** on incubation with Cu^{2+}.

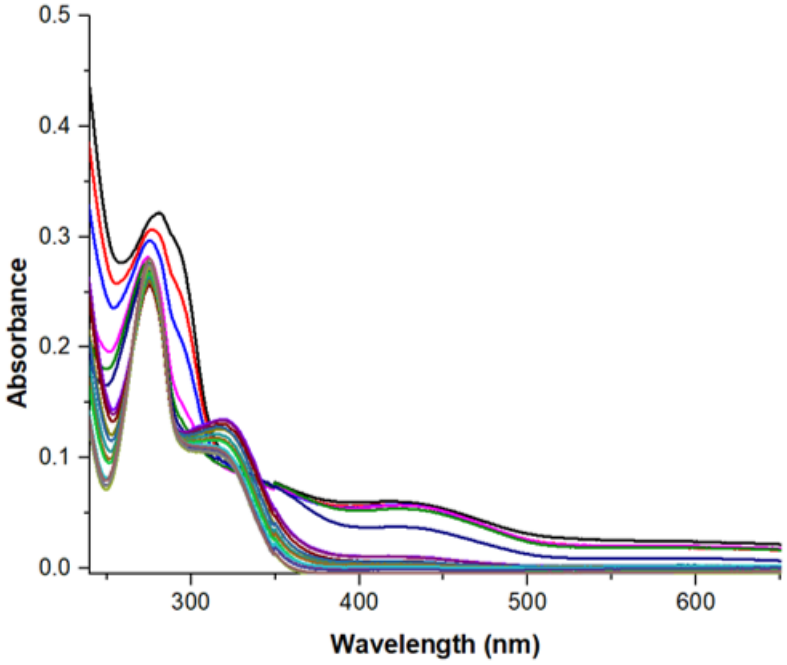

Fig. S3 Absorbance spectra corresponding to the oxidation of pyrocatechol (10 mM) catalysed by increasing concentration of Cu^{2+} in 50 mM HEPES buffer at pH 7.4.

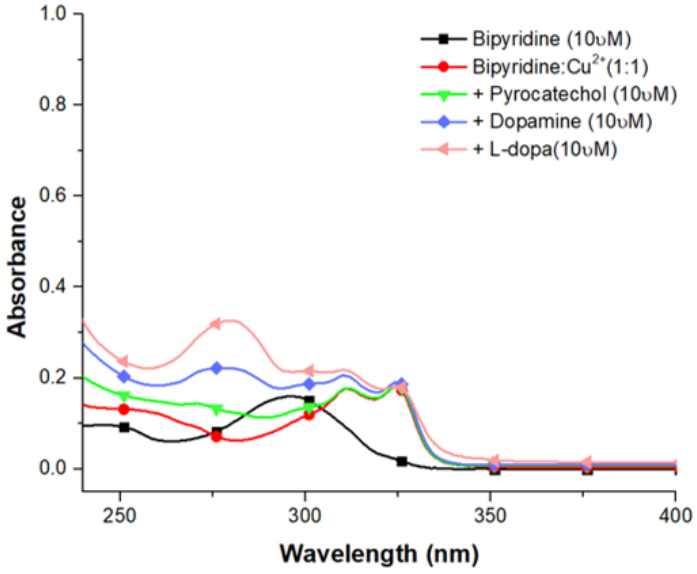

Fig. S4 Absorbance spectra of Cu^{2+} (10μM) binding in presence of bipyridine, pyrocatechol, dopamine, and L-dopa (10μM) in PBS buffer (10 mM , pH 7.4).

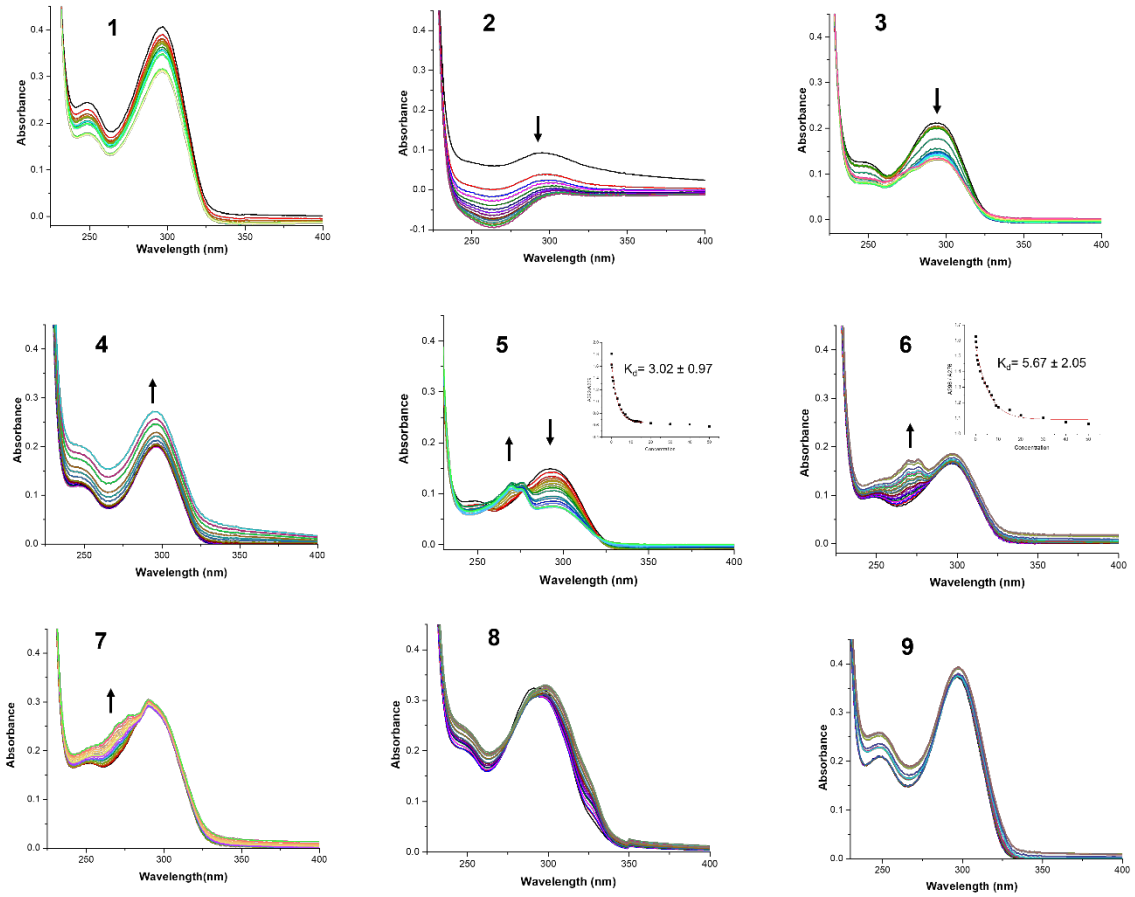

Fig. S5 Zinc ion chelation study. Absorption spectra of compounds **1-9** treated with Zn^{2+} at increasing concentrations of 0.1 µM to 20 µM.

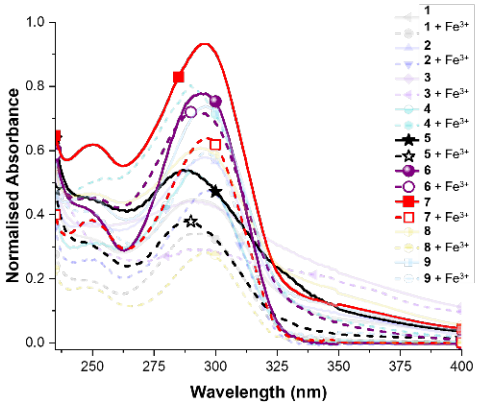

Fig. S6 Metal ion chelation study. Absorption spectra of compounds **1-9** treated with Fe^{3+} at concentrations of 20 µM.

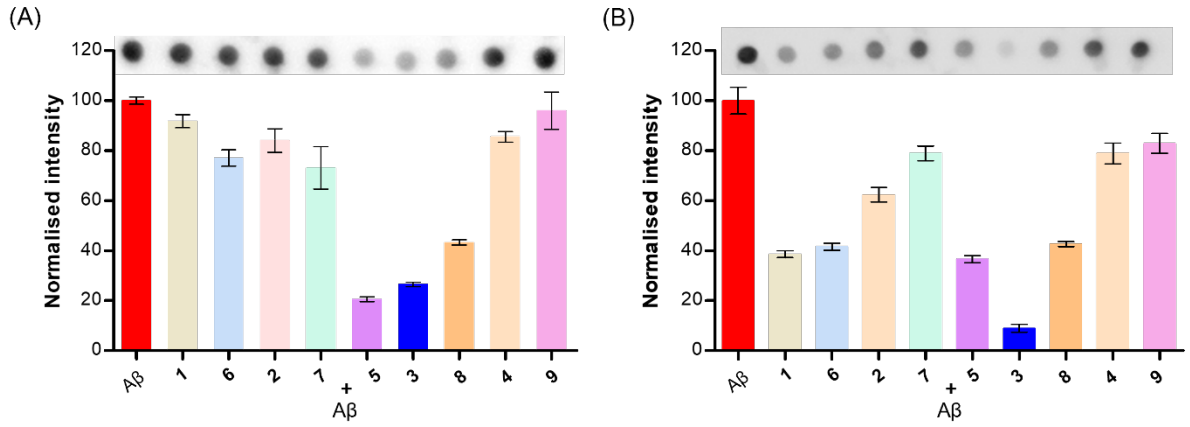

Fig. S7 Dot blot analysis of (A) $A\beta_{42}$ (10 μM) aggregation inhibition and (B) dissolution of preformed $A\beta_{42}$ aggregates by bipyridine compounds **1-9** (5 μM).

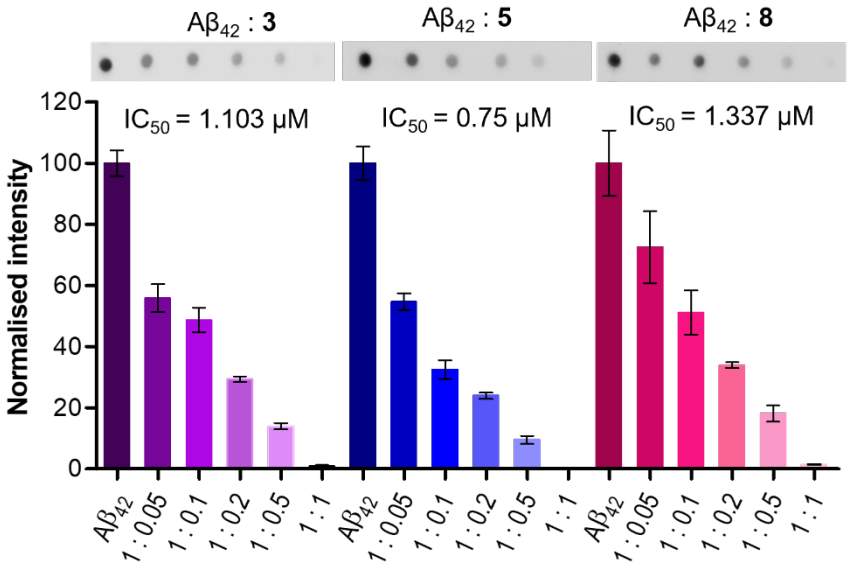

Fig. S8 Dot blot assay and quantification of $A\beta_{42}$ (10 mM) dissolution of preformed fibrils by **3**, **5** and **8** at different molar ratios (1 : 0.05, 1 : 0.1, 1 : 0.2, 1 : 0.5, and 1 : 1).

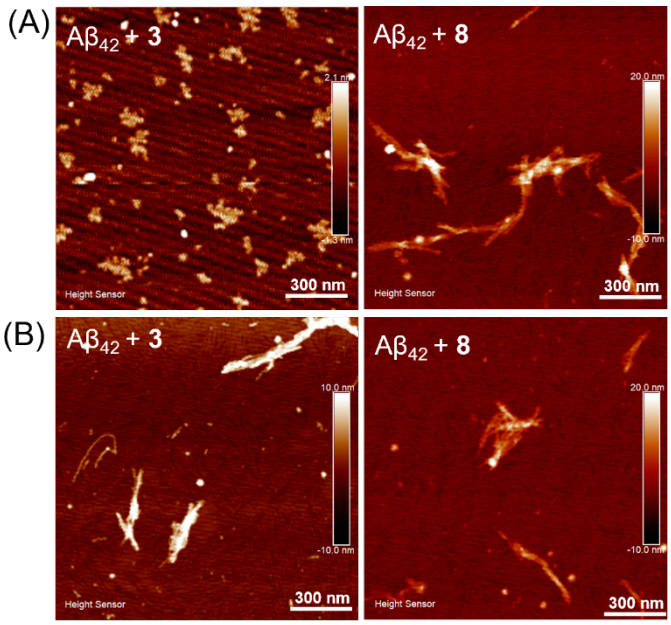

Fig. S9 AFM images of $A\beta_{42}$ alone and with compounds **3** and **8** in (A) aggregation inhibition, and (B) dissolution experiments.

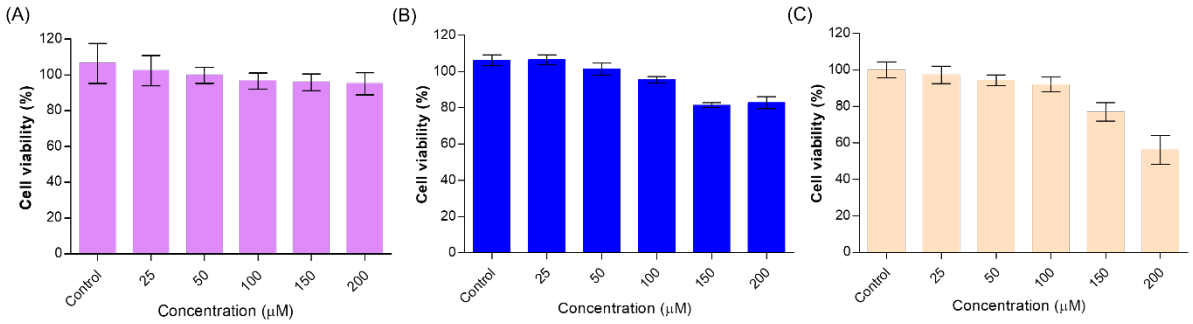

Fig. S10 Cytotoxicity of compounds (A) **3,** (B) **5** and (C) **8** at different concentration from 25 to 200 μM, assessed by MTT assay.

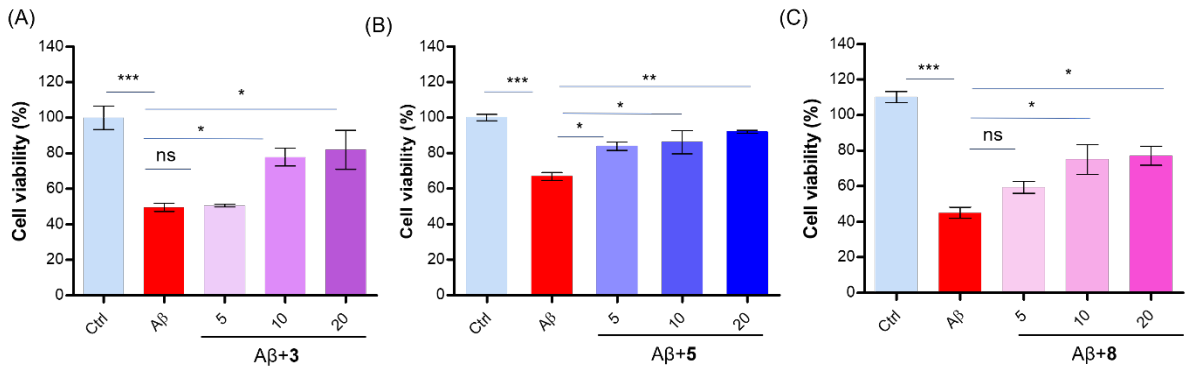

Fig. S11 Neuronal cell rescue from $A\beta_{42}$ toxicity by (A) **3,** (B) **5** and (C) **8,** assessed by MTT assay at different concentration from 5, 10 and 20 µM. (Experiments were repeated with n=4 and statistics was performed with simple One-way ANOVA * p=0.05).

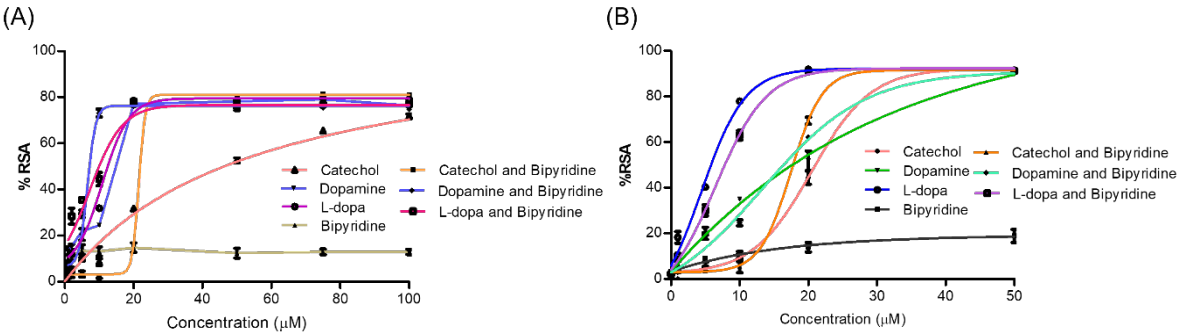

Fig. S12 Radical scavenging activity (RSA) of pyrocatechol, dopamine, L-dopa, bipyridine and their combinations (physical mixture) by (A) DPPH and (B) ABTS assay.

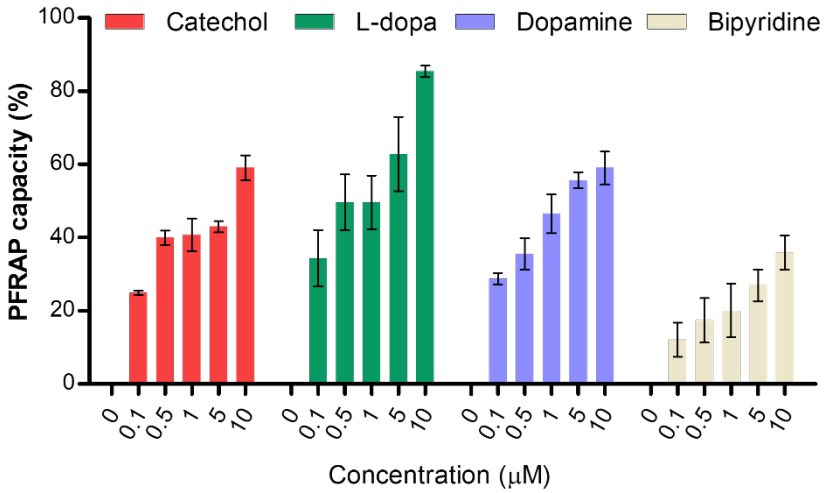

Fig. S13 Quantification of Fe^{3+} reducing ability of pyrocatechol, L-dopa, dopamine and bipyridine at different concentrations (0.1 μM to 10 μM) by PFRAP assay.

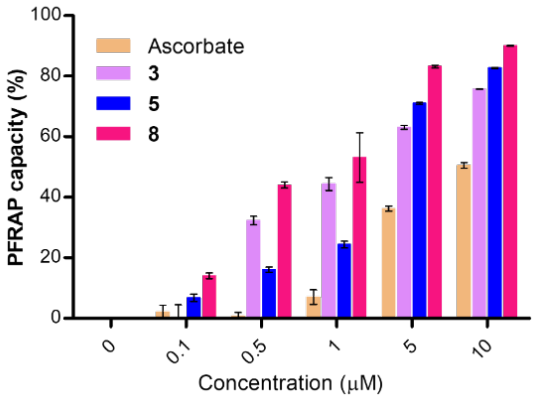

Fig. S14 Quantification of Fe^{3+} reducing ability of compounds **3**, **5** and **8** at different concentrations (0.1 μM to 10 μM) by PFRAP assay.

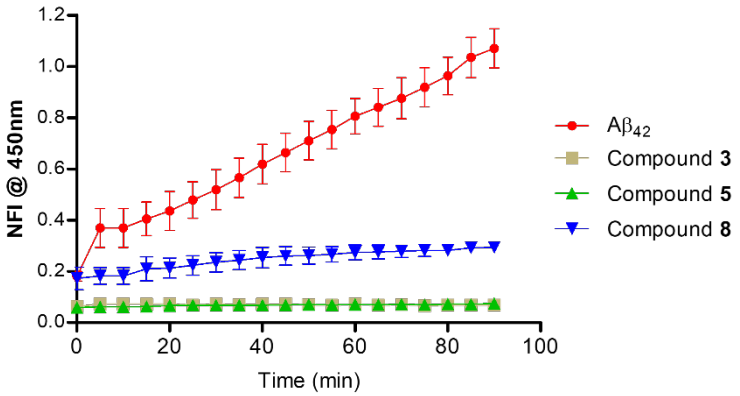

Fig. S15 Normalized fluorescence intensity (NFI) plot of 7-OH-CCA (λ_{em} = 450 nm) containing Cu^{2+}-Aβ42 system as function of time in the absence (control) and presence of compounds **3**, **5** and **8** at 37 °C.

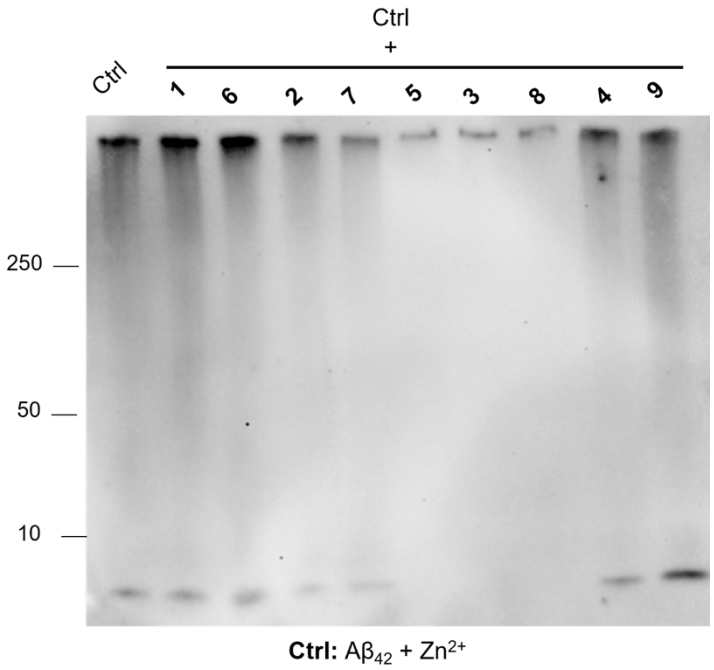

Fig. S16 Native PAGE and western blotting to visualize Aβ42 aggregation inhibition by bipyridine compounds **1**-**9**. Conditions: [Aβ42] = 10 μM, [Zn^{2+}] = 10 μM; [compound] = 10 μM; 24 h, HEPES buffer, pH 6.6 (for Zn^{2+} treated experiments).

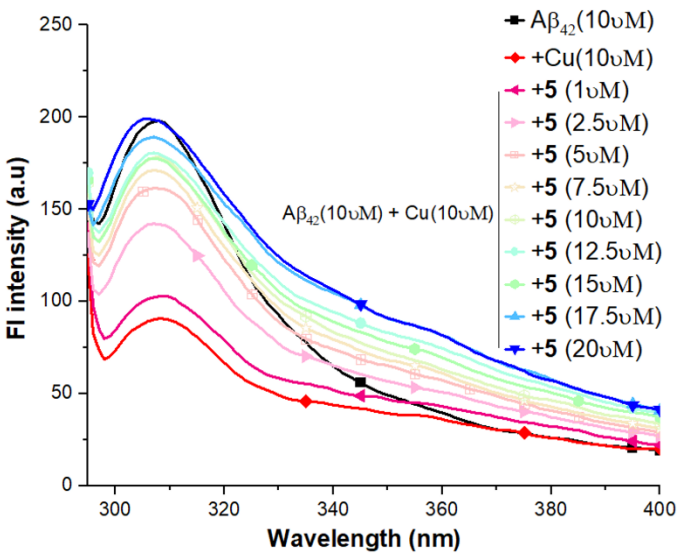

Fig. S17 Fluorescence spectra of Aβ42 (10 mM) in the presence of Cu^{2+} (10 mM) on increasing concentration of compound **5** in 10 mM PBS buffer at pH 7.4.

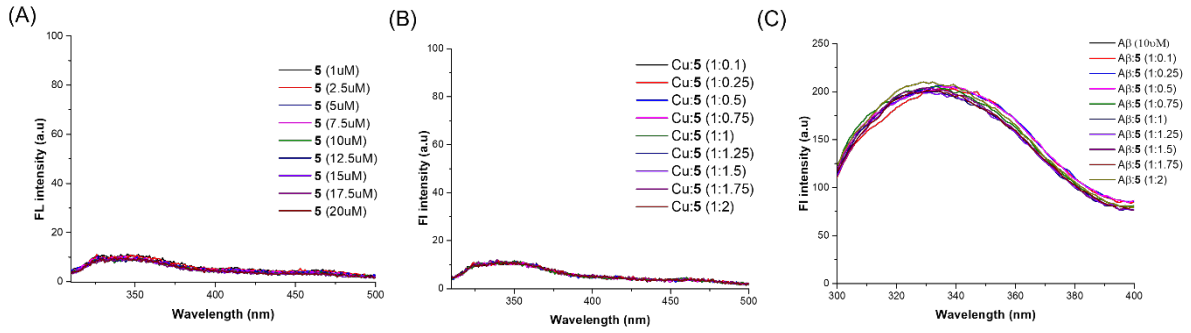

Fig. S18 Fluorescence spectra of (A) compound **5** at different concentrations (1 µM to 20 µM) and (B) on presence of Cu^{2+} (10 µM). (C) Fluorescence spectra of Aβ42 (10 µM) on increasing concentration of compound **5** in PBS buffer (10 mM, pH 7.4).

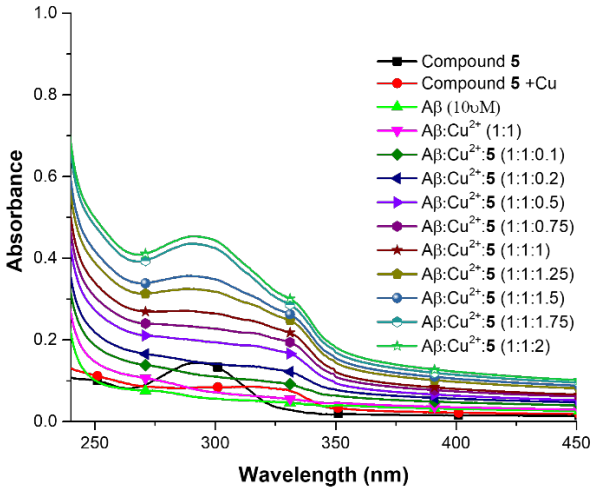

Fig. S19 Absorbance spectra of $A\beta_{42}$ (10 μM) in the presence of Cu^{2+} (10 μM) on increasing concentration of compound **5**, in PBS buffer (10 mM , pH 7.4).

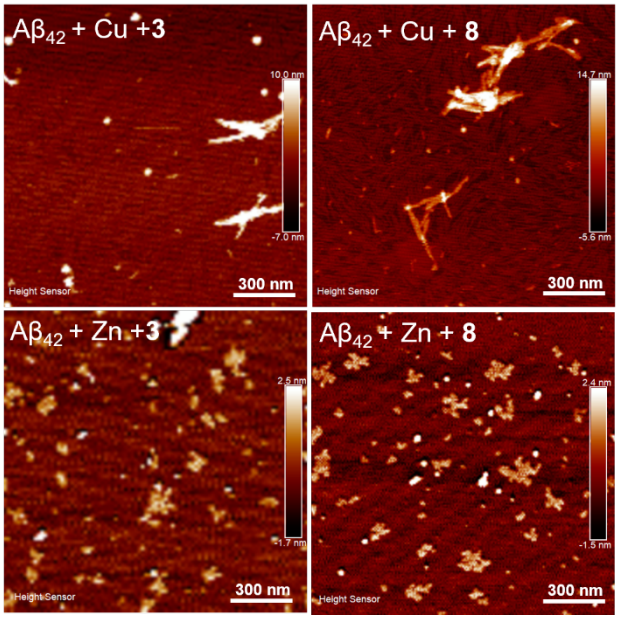

Fig. S20 AFM images of metal-dependent (Cu and Zn) $A\beta_{42}$ aggregation inhibition by compounds **3** and **8**.

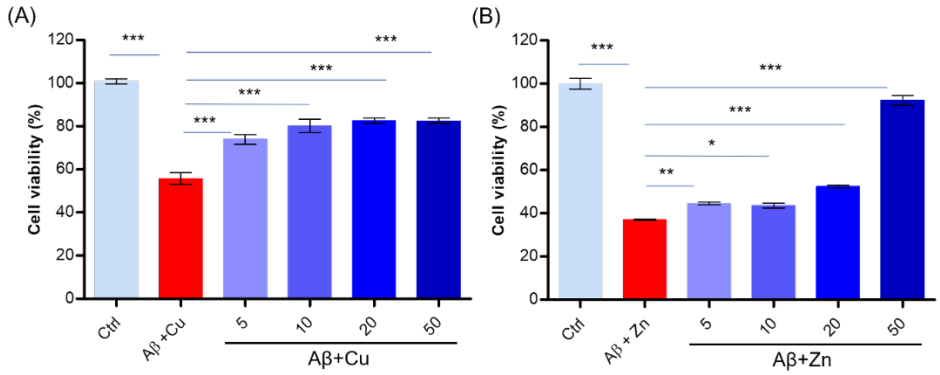

Fig. S21 Cell rescue from (A) Cu and (B) Zn dependent $A\beta_{42}$ toxicity by compound **5** at different concentrations (5, 10, 20 and 50 μM).

^{1}H, ^{13}C and HRMS of bipyridine compounds 1-9

^{1}H NMR spectrum of **1** (400 MHz, DMSO-d_6)

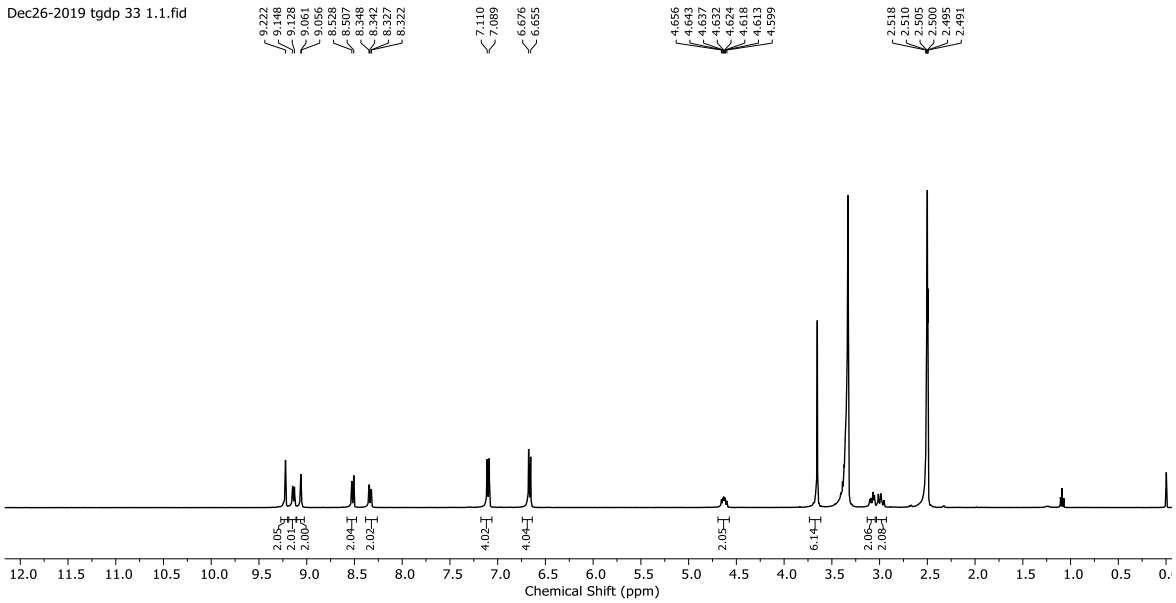

^{13}C NMR spectrum of **1** (100 MHz, DMSO-d_6)

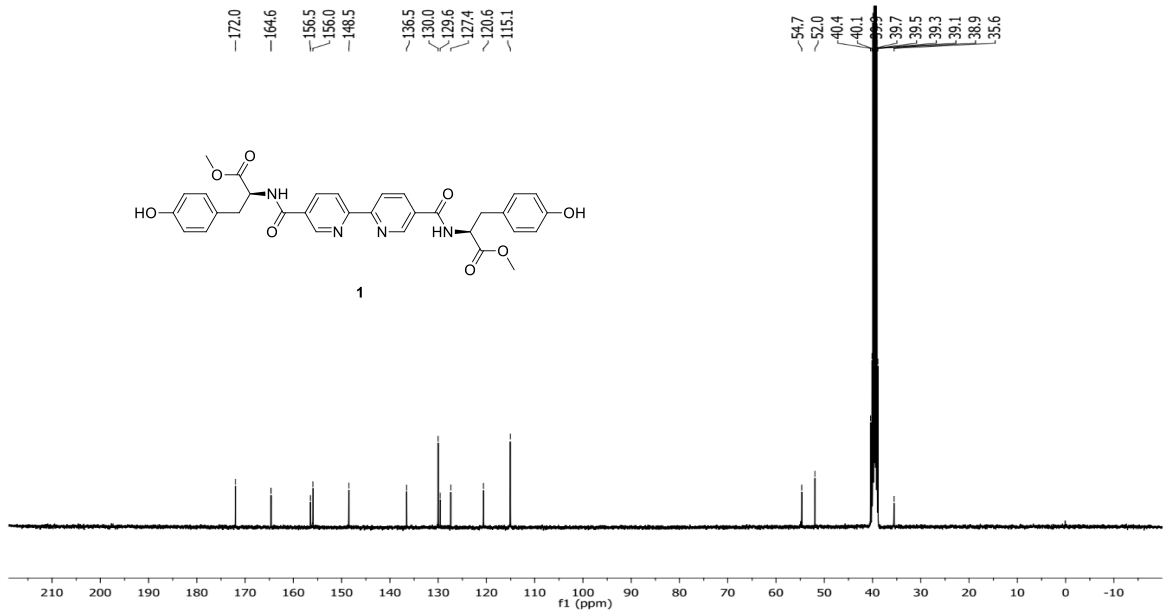

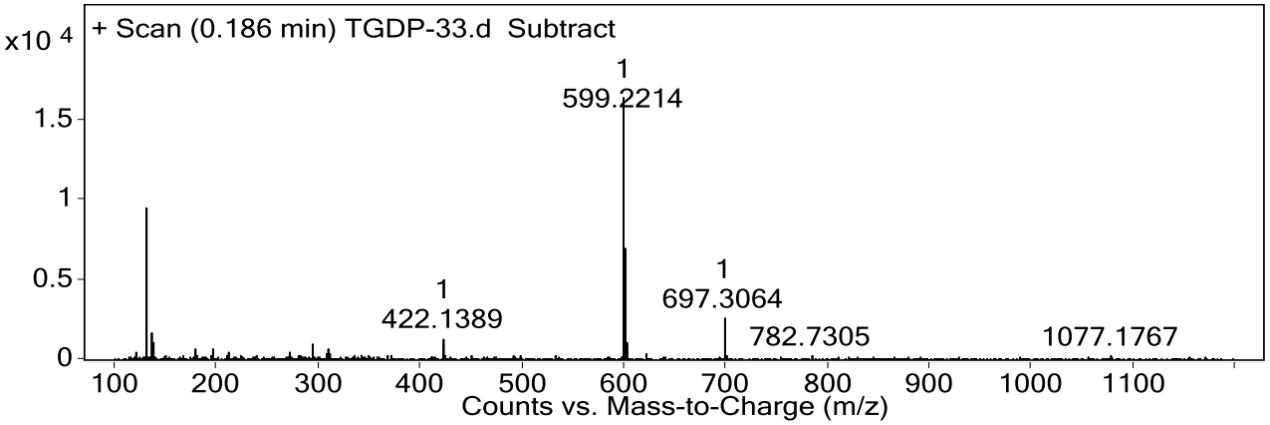

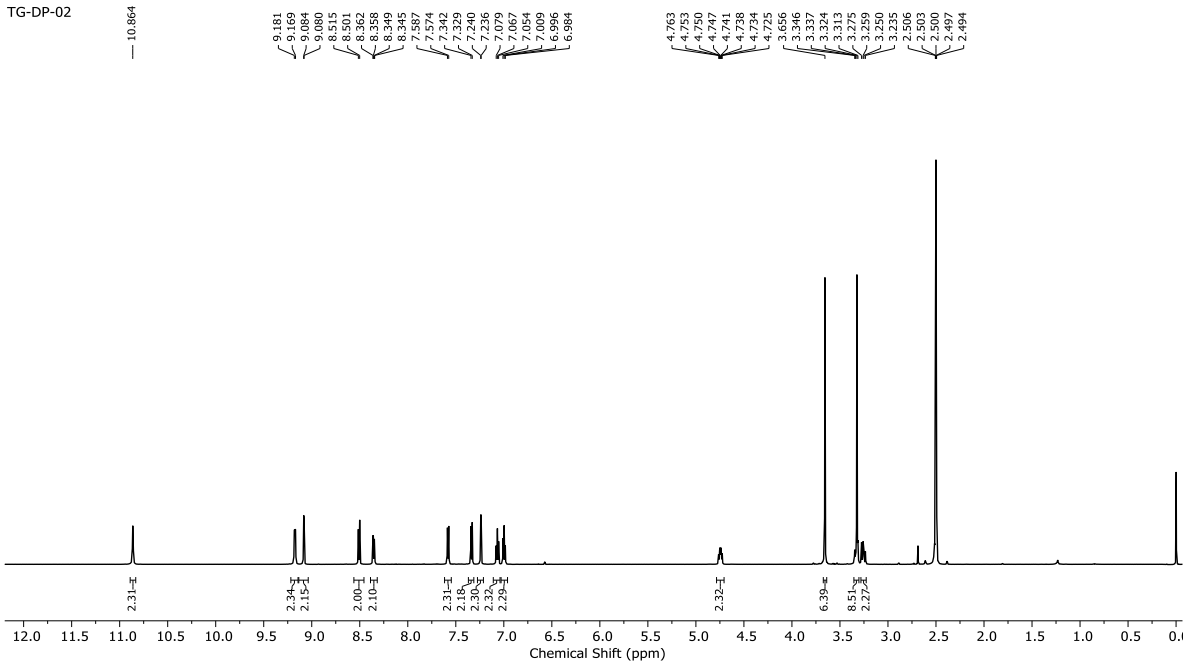

^{13}C NMR spectrum of **2** (100 MHz, DMSO-d_6)

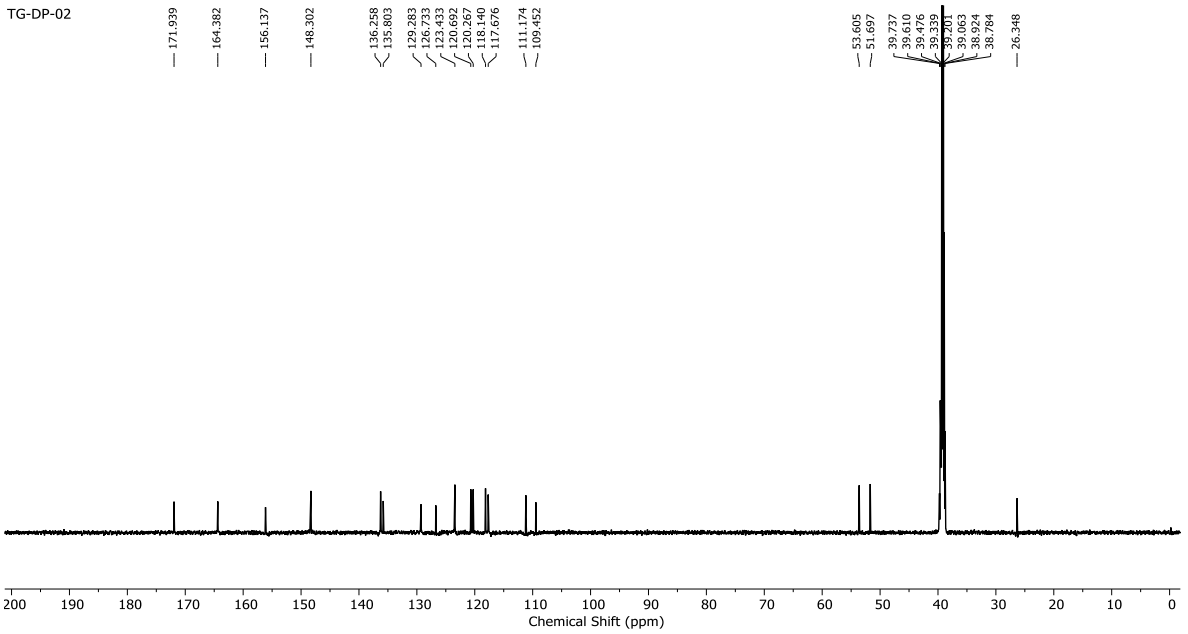

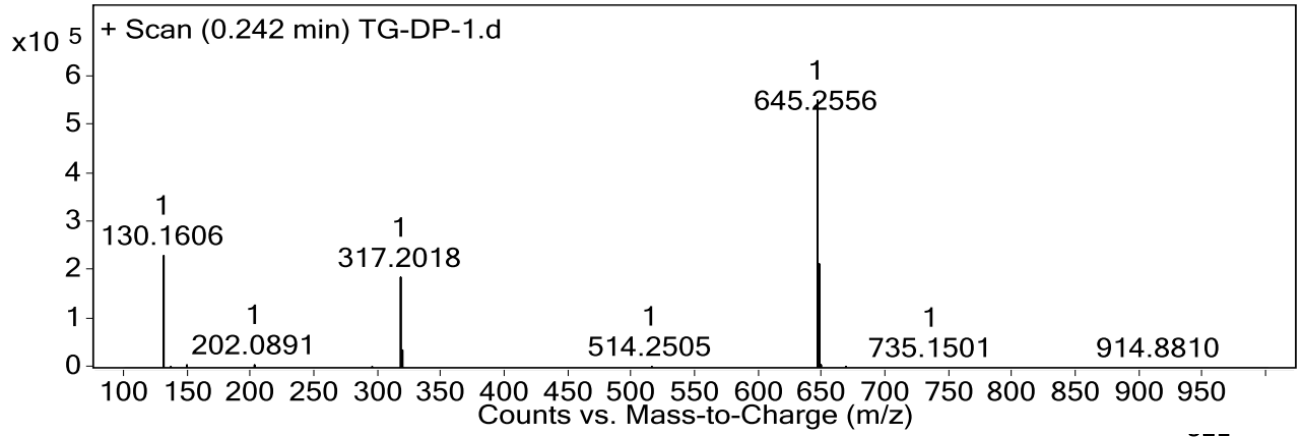

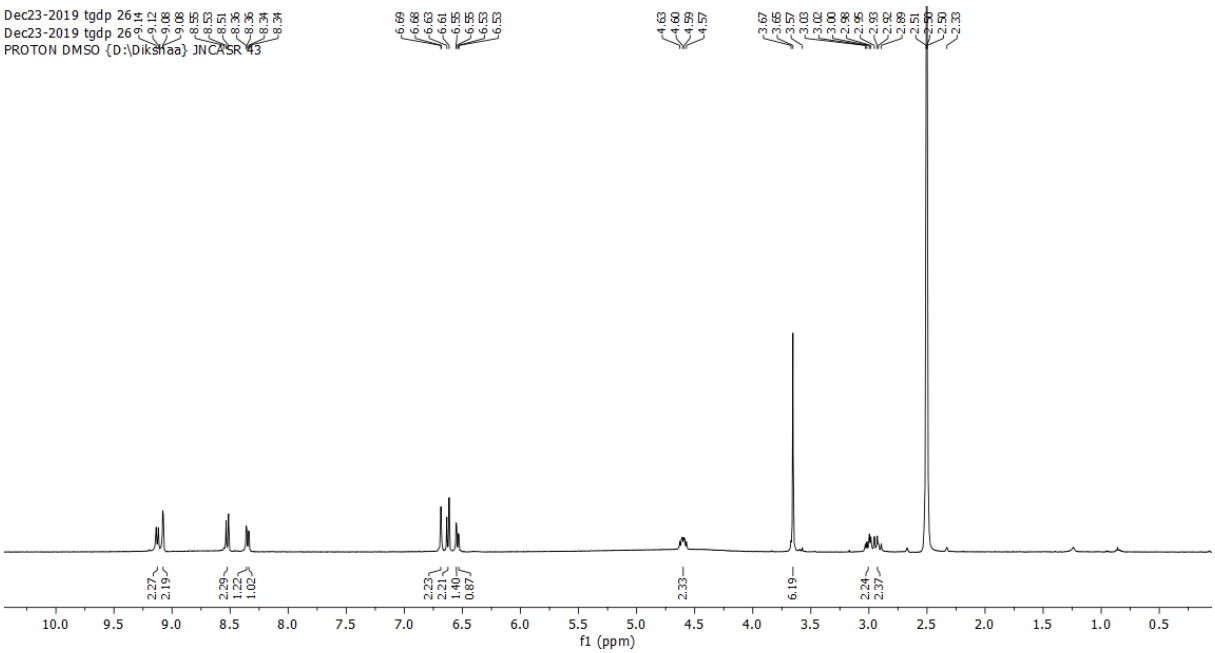

^{13}C NMR spectrum of **3** (100 MHz, DMSO-d_6)

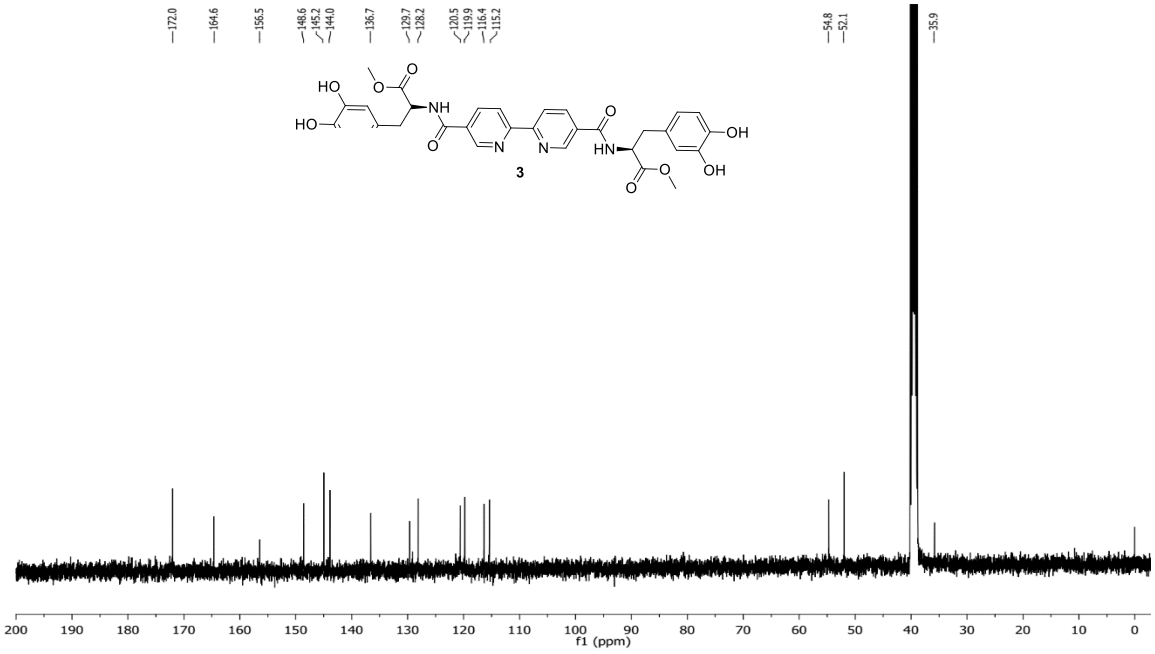

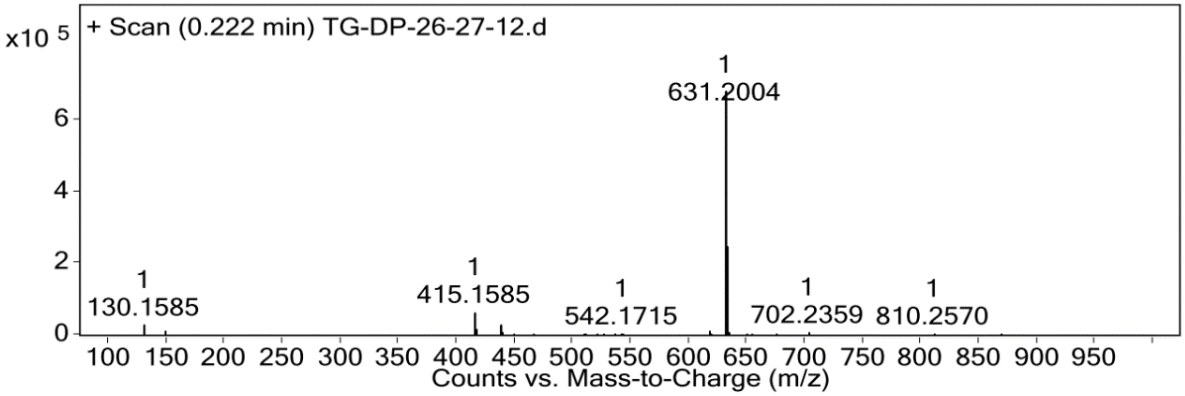

^{1}H NMR spectrum of **4** (400 MHz, DMSO-d_6)

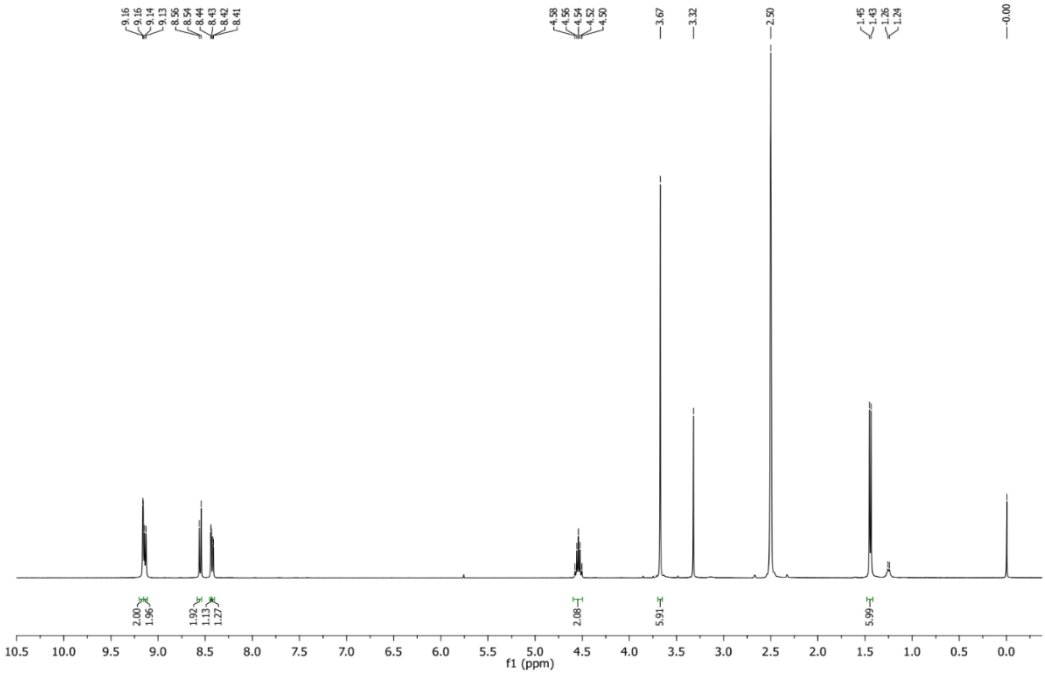

^{13}C NMR spectrum of **4** (100 MHz, DMSO-d_6)

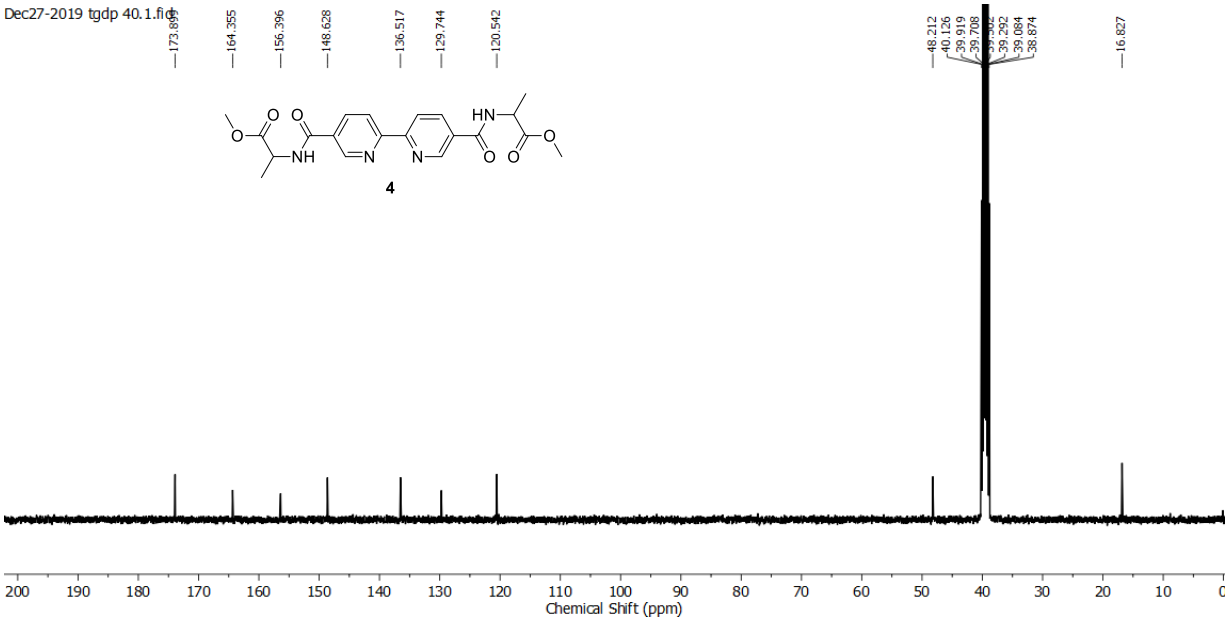

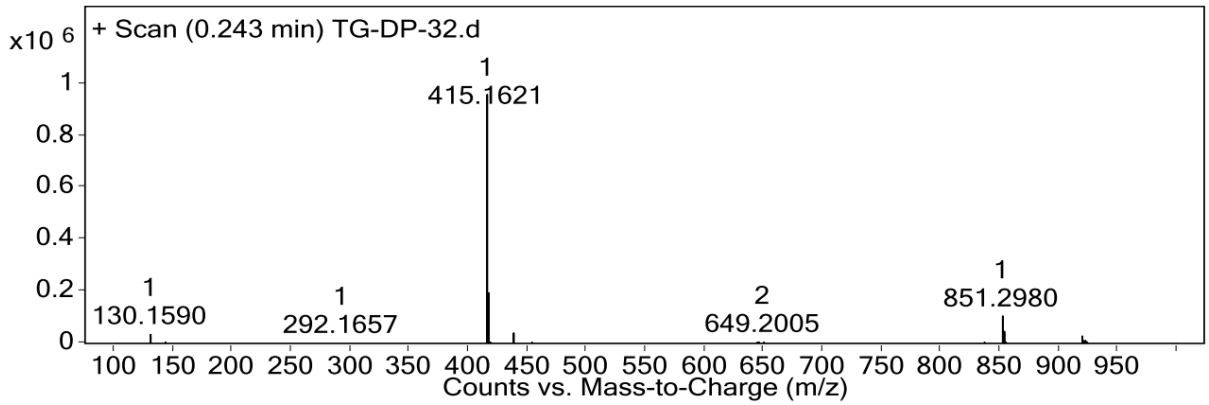

^{1}H NMR spectrum of **5** (400 MHz, DMSO-d_6)

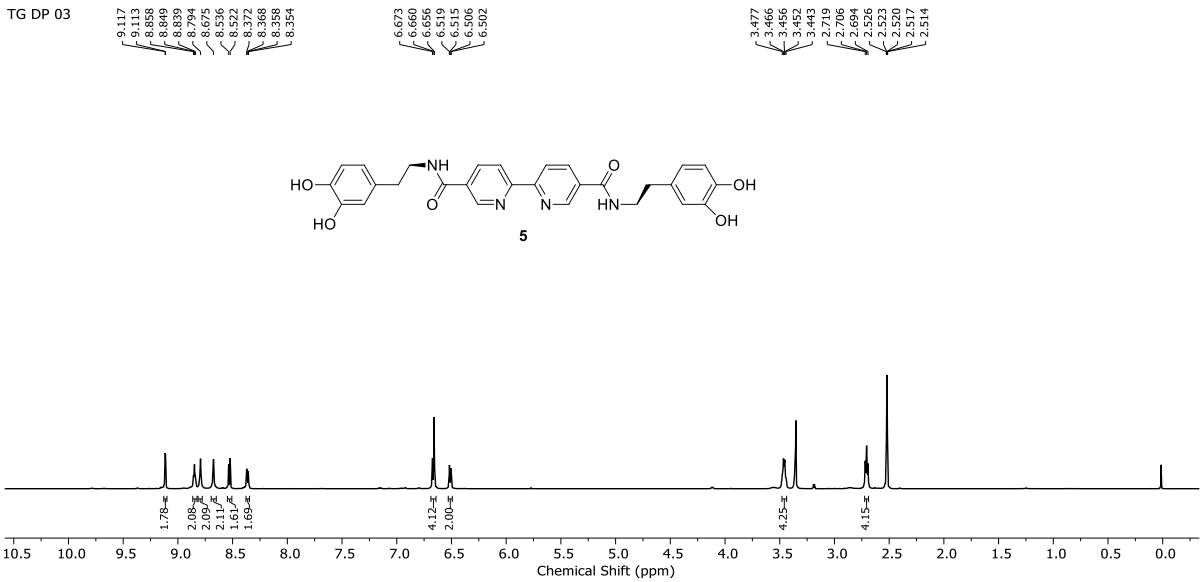

^{13}C NMR spectrum of **5** (100 MHz, DMSO-d_6)

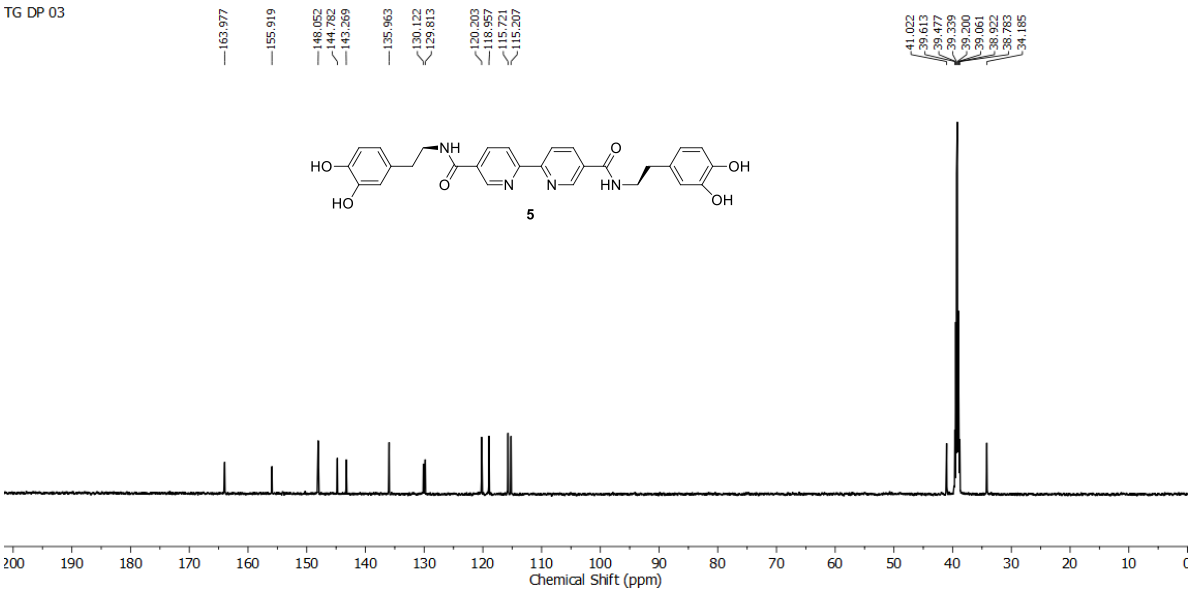

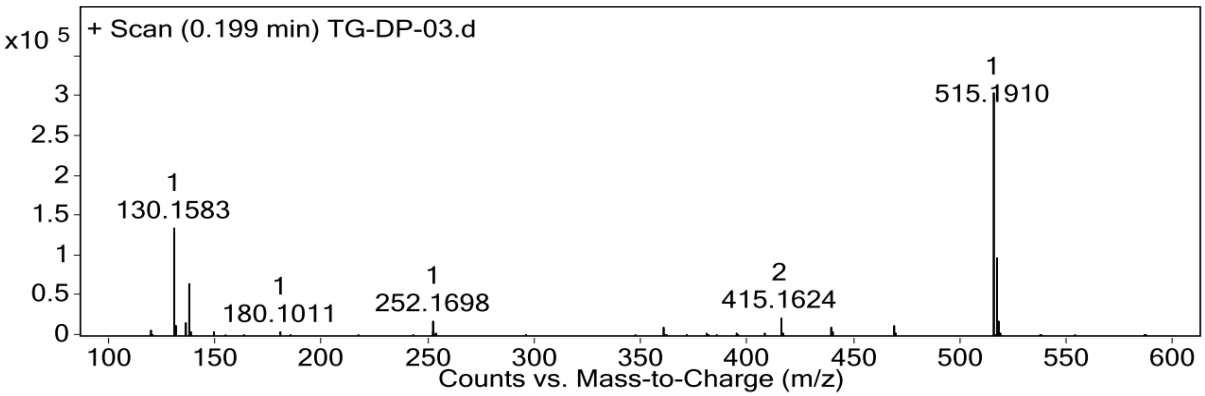

^{1}H NMR spectrum of **6** (400 MHz, DMSO-d_6)

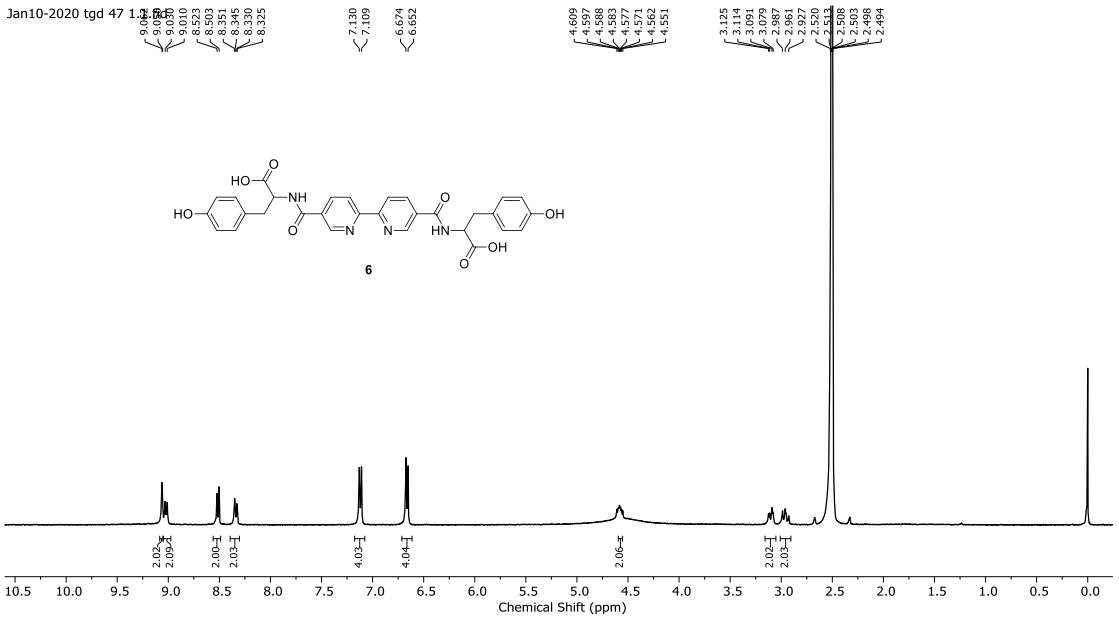

^{13}C NMR spectrum of **6** (100 MHz, DMSO-d_6)

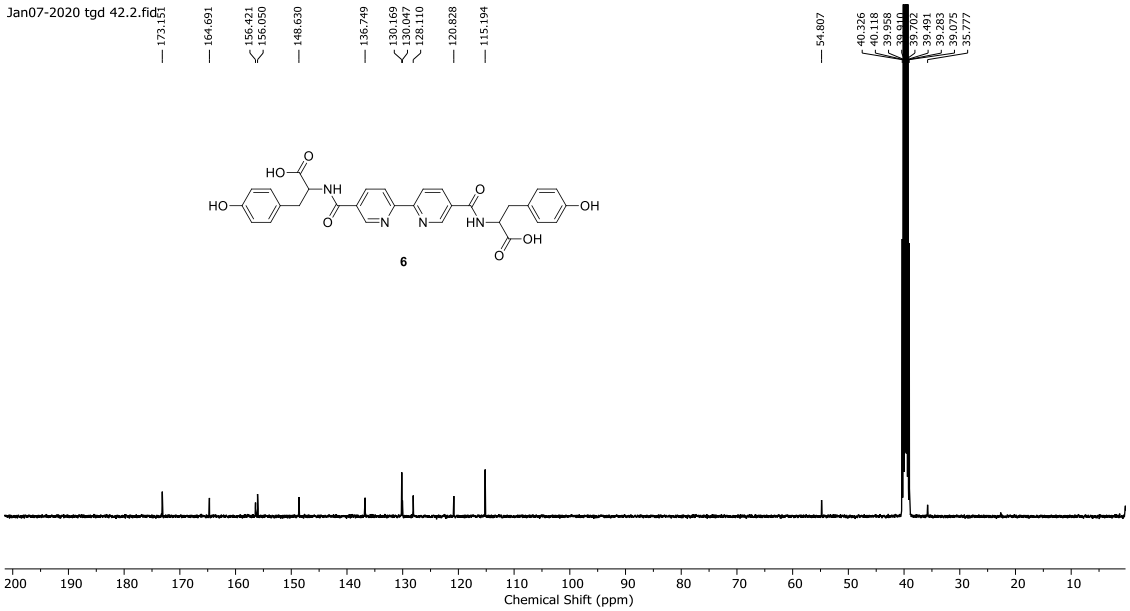

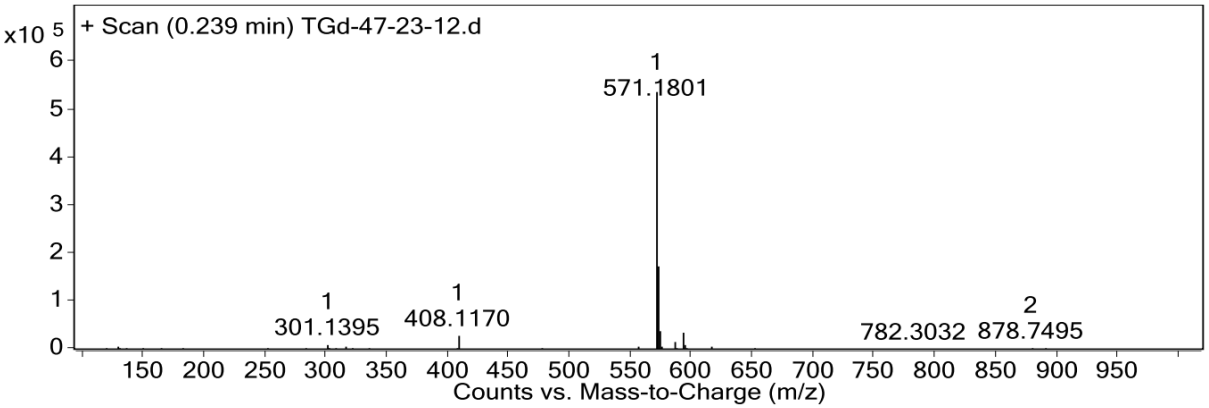

^{1}H NMR spectrum of **7** (400 MHz, DMSO-d_6)

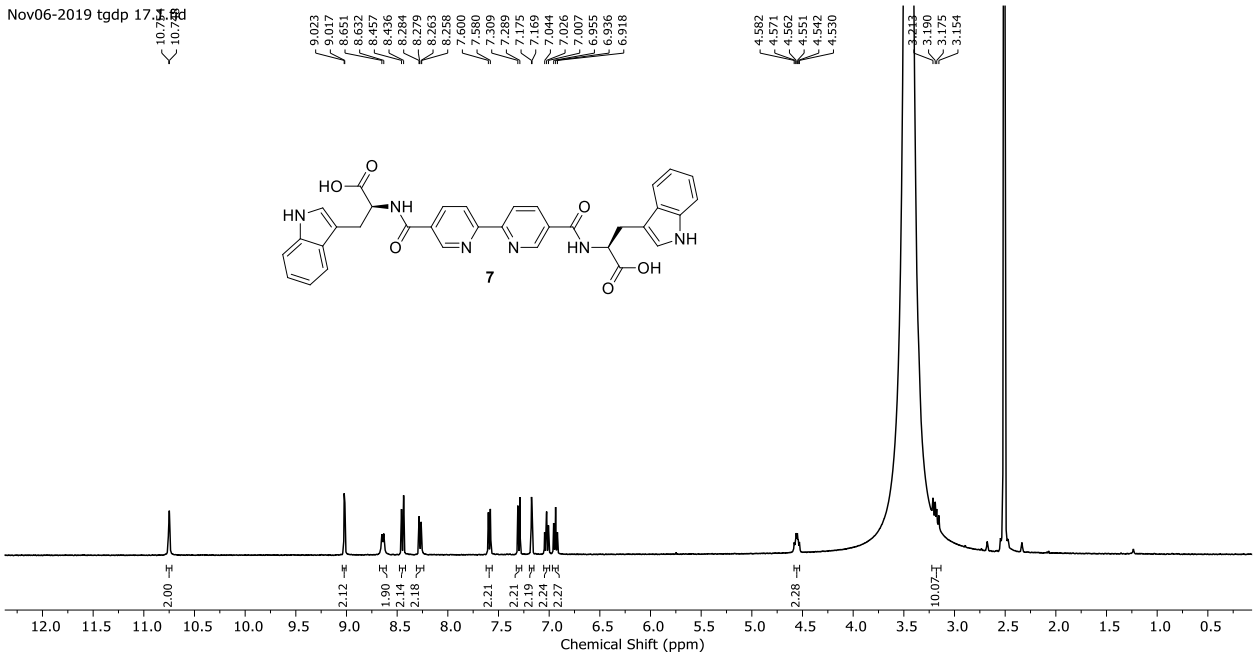

^{13}C NMR spectrum of **7** (100 MHz, DMSO-d_6)

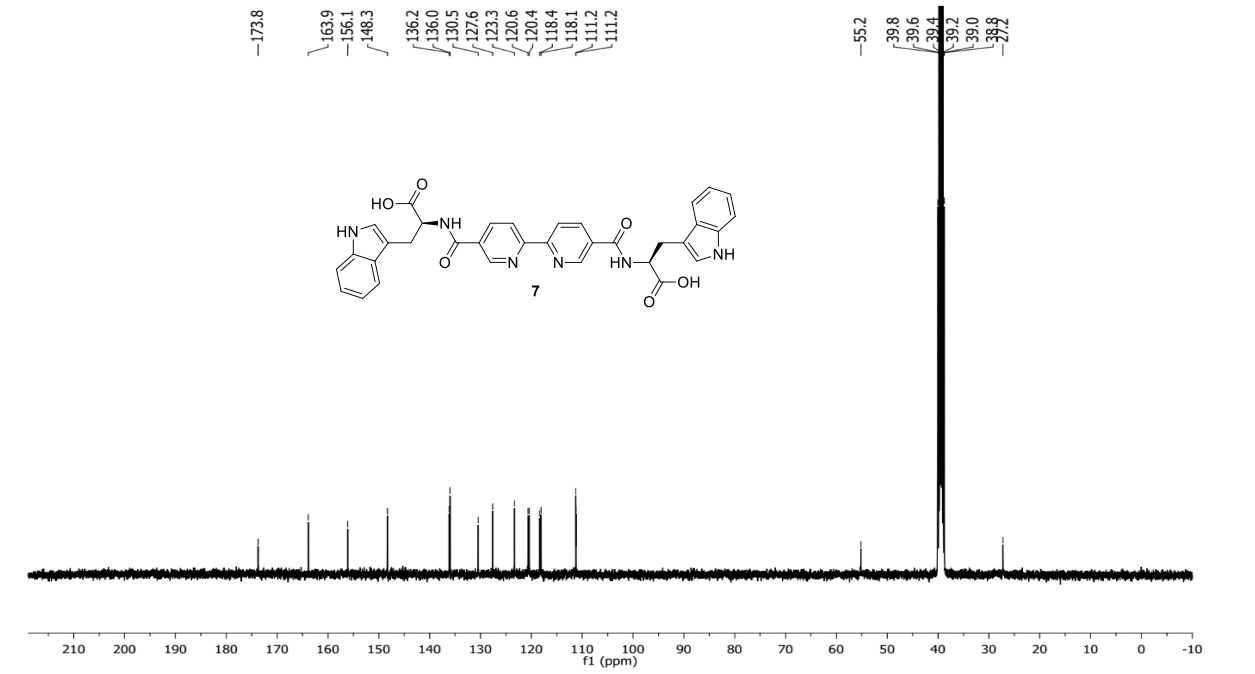

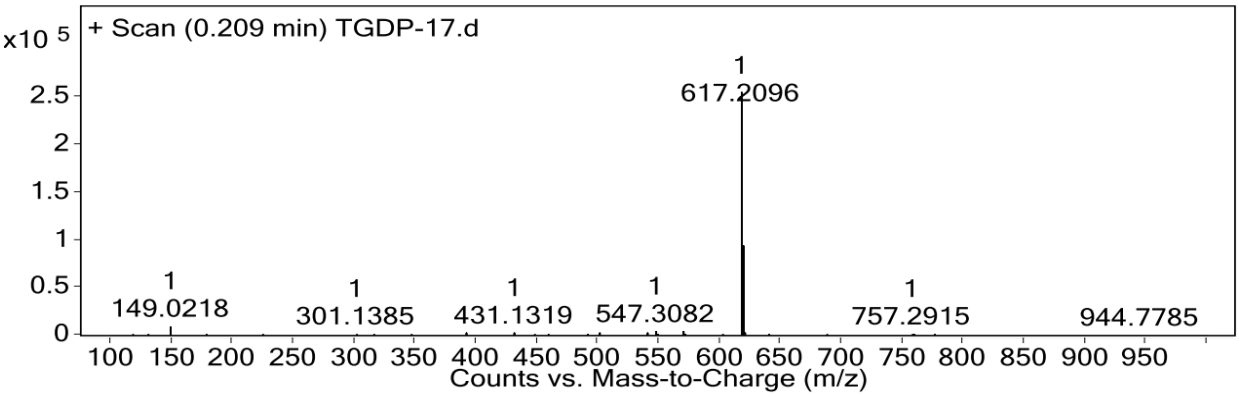

^{1}H NMR spectrum of **8** (400 MHz, DMSO-d_6)

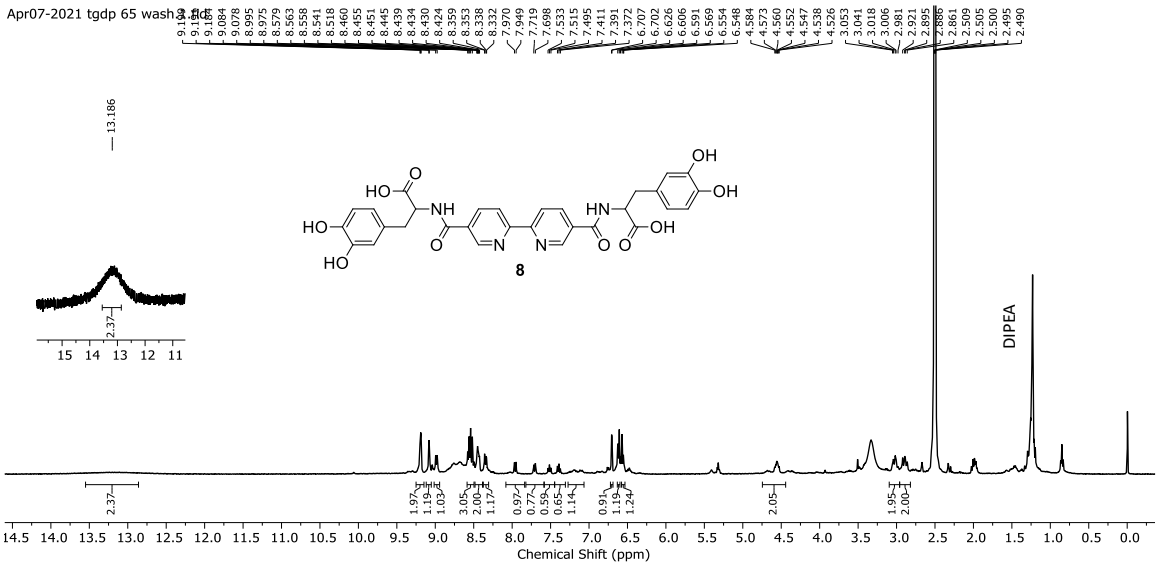

^{13}C NMR spectrum of **8** (100 MHz, DMSO-d_6)

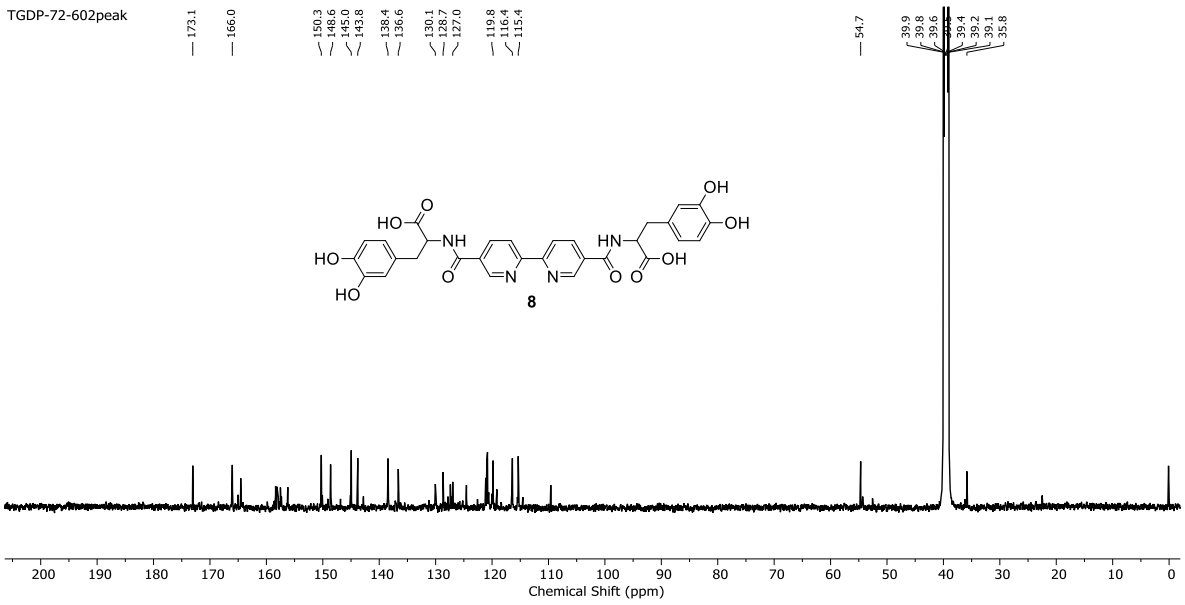

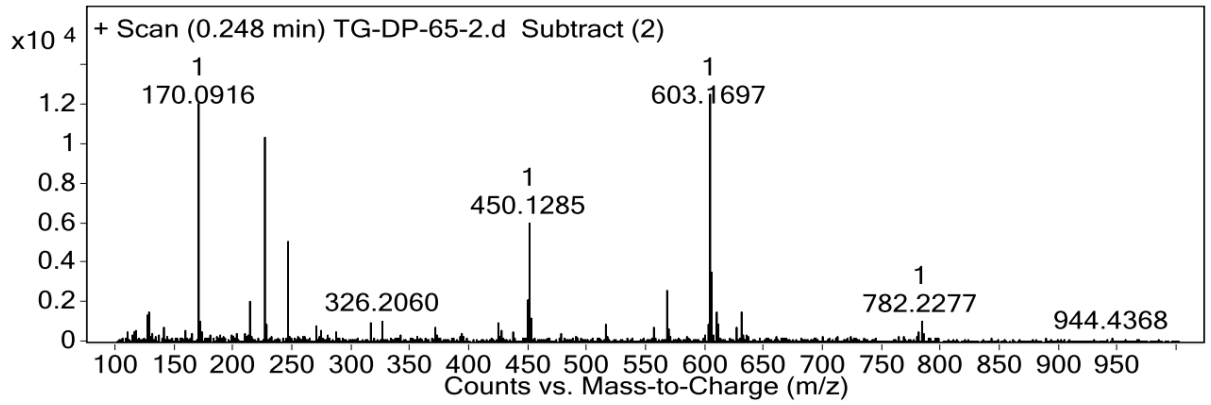

^{1}H NMR spectrum of **9** (400 MHz, DMSO-d_6)

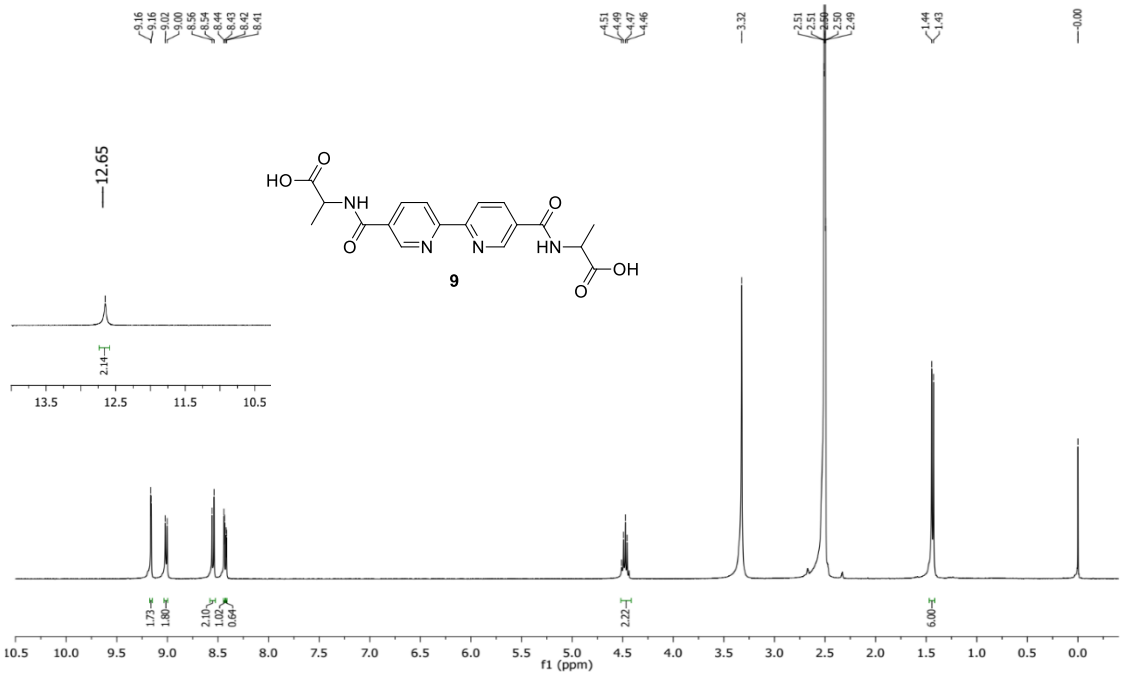

^{13}C NMR spectrum of **9** (100 MHz, DMSO-d_6)

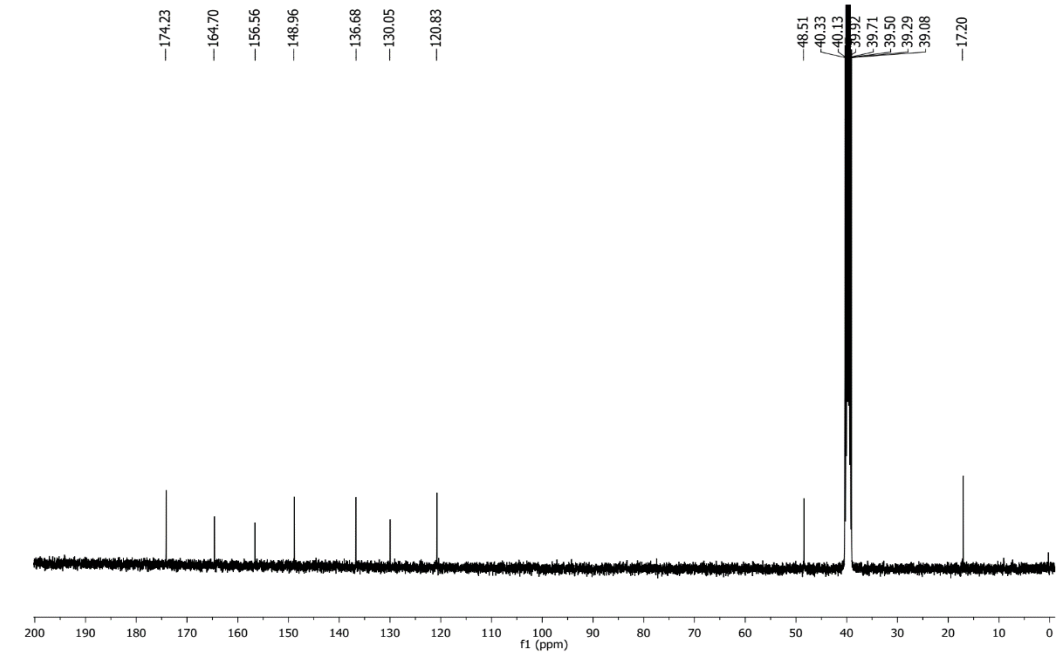

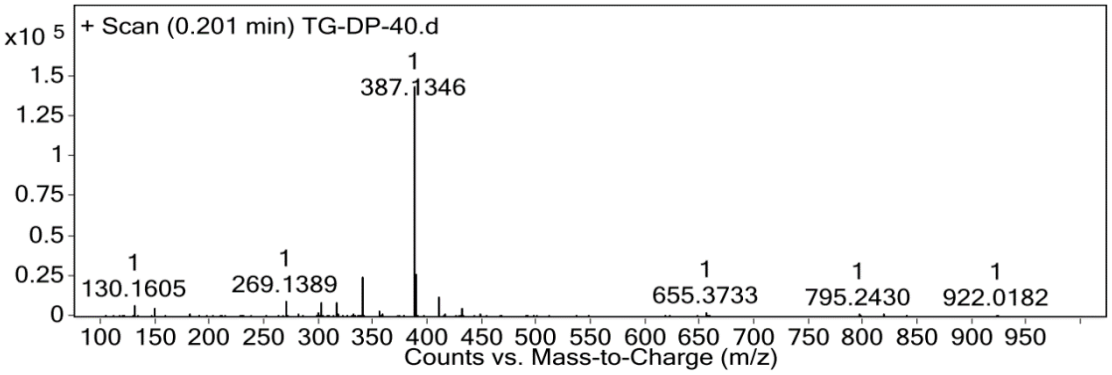

References

1 C. Bacchella, S. Dell'acqua, S. Nicolis, E. Monzani and L. Casella, *Int. J. Mol. Sci.*, 2021, **22**, 5190. DOI:10.3390/ijms22105190.